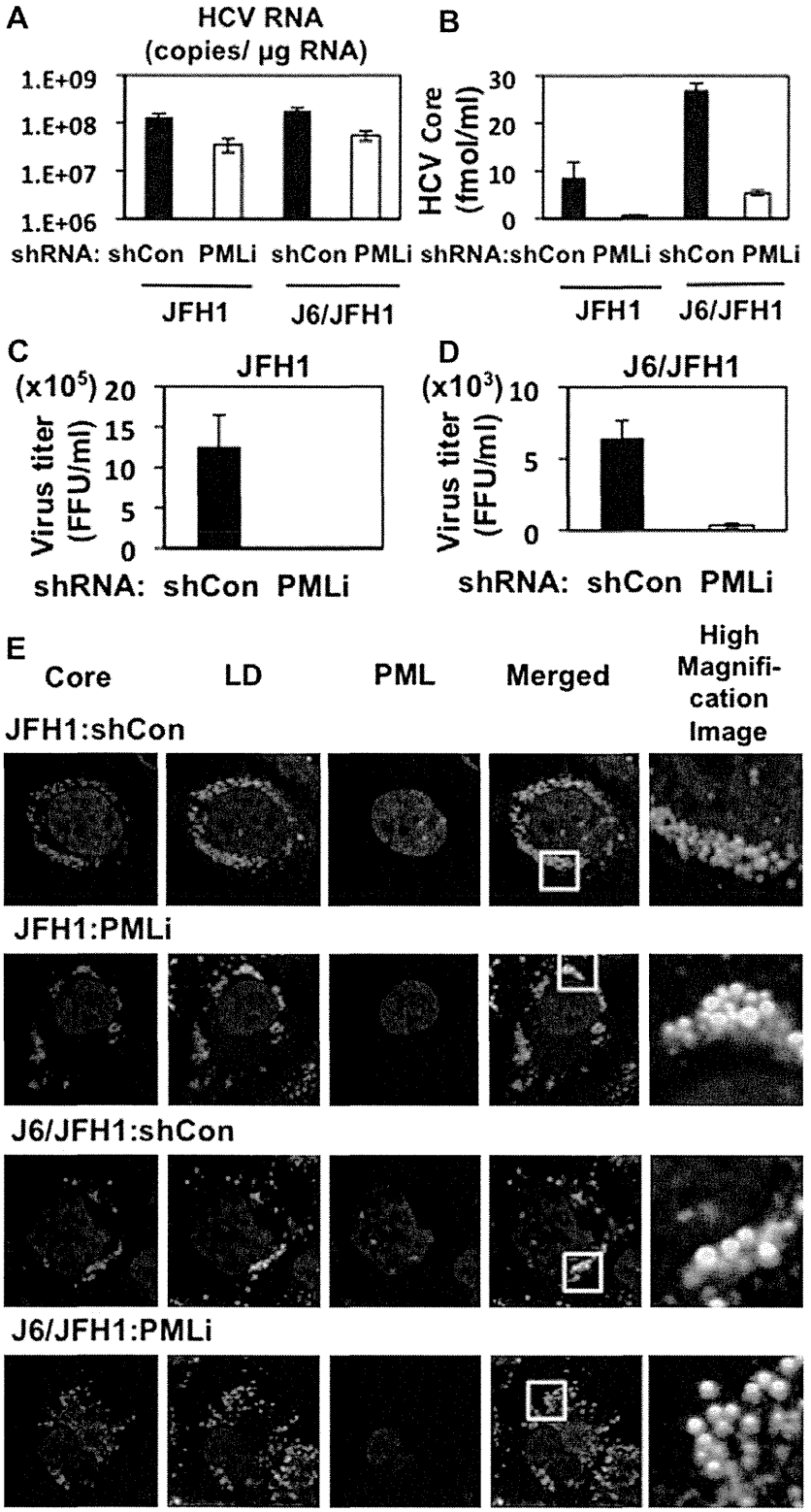

Fig. 3. PML is dispensable for the localization of HCV core to lipid droplet. (A) The levels of intracellular HCV RNA in PML knockdown or the control RSc cells 96 h after inoculation of HCV-JFH1 or HCV-J6/JFH1 were monitored by real-time LightCycler RT-PCR. Results from three independent experiments are shown (A–C). (B) The levels of HCV core in the culture supernatants from the PML knockdown RSc cells at 96 h post-infection were determined by ELISA. (C, D) The infectivity of HCV in the culture supernatants was determined by a focus-forming assay at 48 h post-infection. (E) HCV core localizes to lipid droplet (LD) in the PML knockdown (PMLi) or the control (shCon) cells after infection with either HCV-JFH1 or HCV-J6/JFH1. Cells were fixed 72 h post-infection and were then examined by confocal laser scanning microscopy.

3.2. PML is unrelated to HCV RNA replication

To examine whether or not PML is involved in HCV RNA replication, we used the subgenomic replicon RNA of HCV-JFH1, JRN/3-5B, encoding *Renilla* luciferase gene for monitoring the HCV RNA replication (Fig. 2A). *In vitro* transcribed JRN/3-5B RNA was transfected into the PML knockdown OR6c cells by electroporation and we examined the luciferase activity. Consequently, the

luciferase activity in the PML knockdown cells was similar to that of the control cells (Fig. 2B), indicating that shRNA targeted to PML could not affect the transient HCV RNA replication. As well, the level of HCV RNA in PML knockdown HuH-7-derived OR6c JRN/3-5B cells harboring the subgenomic replicon RNA of HCV-JFH1 and the cell growth was not affected (Fig. 2C and D), suggesting that PML is unrelated to the HCV RNA replication. To further confirm whether or not PML is involved in HCV production, we used *trans*-packaging system [21,22], that HCV subgenomic replicon was efficiently encapsidated into infectious virus-like particles by expression of HCV core to NS2 coding region. In fact, infectious HCV-like particles were produced and released into the culture medium from PML knockdown JRN/3-5B cells stably expressing core to NS2 coding region of HCV-JFH1 genome by mouse retroviral vector (Fig. 2E). We could monitor the HCV RNA replication by *Renilla* luciferase assay in target naïve RSc cells after the inoculation of infectious HCV-like particles. Consequently, the release of infectious HCV-like particles into the culture supernatants was significantly suppressed in PML knockdown cells at 72 h post-infection (Fig. 2F). Thus, we conclude that PML is associated with HCV production.

3.3. PML is required for the late step in the HCV-JFH1 life cycle

To avoid the possibility of specific finding when we only used HCV-JFH1, we examined another strain of HCV-J6JFH1 [20]. For this, we analyzed the level of HCV core and the infectivity in the culture supernatant as well as the level of HCV RNA in the PML knockdown RSc cells 96 h after inoculation of HCV-J6/JFH1. In this context, the level of HCV RNA in PML knockdown cells was only somewhat decreased (Fig. 3A), while the level of core and the infectivity in the culture supernatants was remarkably reduced (Fig. 3B–D), indicating that PML is required for infectious HCV-J6/JFH1 production as well as HCV-JFH1.

Since lipid droplets have been shown to be involved in an important cytoplasmic organelle for HCV production [3], we performed immunofluorescence and confocal microscopic analyses to determine whether or not HCV core misses localization into lipid droplets in the PML knockdown cells. We found that the core protein was targeted into lipid droplets even in PML knockdown RSc cells as well as in the control RSc cells after infection with either HCV-JFH1 or HCV-J6/JFH1 (Fig. 3E). This suggests that PML plays a role in the late step after the core is targeted into lipid droplet in the HCV life cycle. Importantly, HCV did not disrupt the formation of PML-NBs in response to HCV infection (Fig. 3E) unlike HIV-1 and other DNA viruses [6,7,23].

3.4. INI1 and DDX5, PML-related proteins, are involved in HCV production

Finally, we established the INI1 or DDX5, PML-related protein [23,24], knockdown RSc or OR6c JRN/3-5B cells by lentiviral vector expressing shRNA target to INI1 [17] or DDX5 to examine potential role of INI1 and DDX5 in HCV life cycle. Consequently, we found that the release of HCV core or the infectivity of HCV into the culture supernatants was significantly suppressed in the INI1 or DDX5 knockdown RSc cells 96 h after HCV-JFH1 infection, while the RNA replication in the knockdown cells was only somewhat decreased in spite of the very effective knockdown of INI1 or DDX5 mRNA without growth inhibition (Fig. 4A–F), suggesting that INI1 and DDX5 are involved in HCV life cycle. To confirm whether or not these proteins are involved in HCV RNA replication, we examined the luciferase assay in the INI1 or DDX5 knockdown OR6c JRN/3-5B cells. In this context, the shRNA target to INI1 or DDX5 did not affect the luciferase activity and the cell growth in these knockdown cells (Fig. 4G and H), suggesting that both INI1 and DDX5 are required for HCV production like PML.

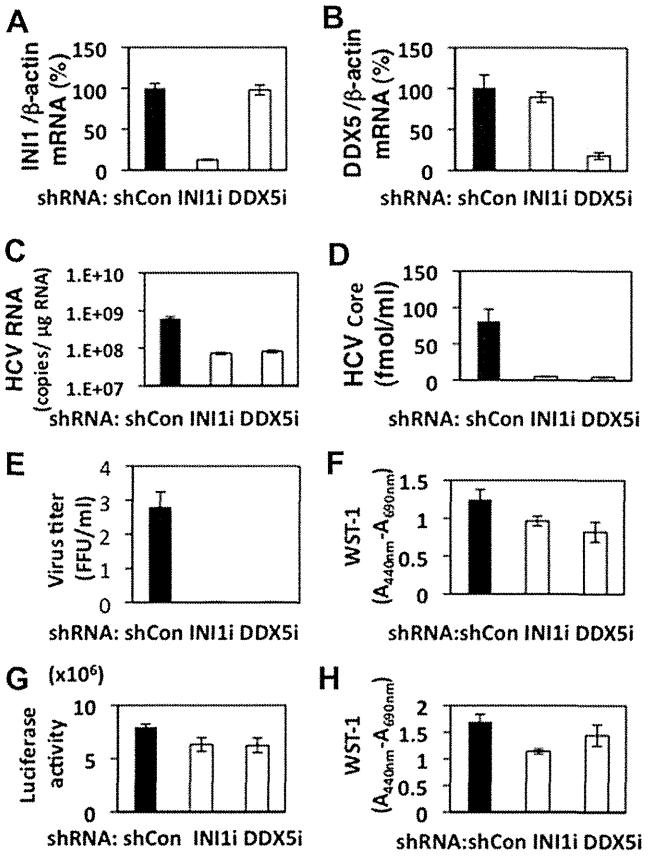

Fig. 4. INI1 and DDX5, PML-related proteins, are required for HCV production. (A, B) Inhibition of INI1 and DDX5 mRNA expressions by the shRNA-producing lentiviral vector. Real-time LightCycler RT-PCR for INI1 and DDX5 was performed as well as for β-actin mRNA in triplicate. Each mRNA level was calculated relative to the level in RSc cells transduced with a control lentiviral vector (Con) which was assigned as 100%. (C) The levels of intracellular genome-length HCV-JFH1 RNA in each knockdown cells at 96 h post-infection at an MOI of 0.05 were monitored by real-time LightCycler RT-PCR. (D) The levels of HCV core in the culture supernatants from the INI1 (INI1i) or DDX5 knockdown (DDX5i) RSc cells 96 h after inoculation of HCV-JFH1 were determined by ELISA. (E) The infectivity of HCV-JFH1 in the culture supernatants was determined by a focus-forming assay at 48 h post-infection. Virus titer is shown as ($x10^7$) FFU/ml. (F) WST-1 assay of each knockdown RSc cells at 96 h post-infection. (G) The HCV RNA replication level in INI1 and DDX5 knockdown OR6c JRN/3-5B cells was monitored by RL assay. (H) WST-1 assay of each knockdown OR6c JRN/3-5B cells. All results shown are means from three independent experiments.

4. Discussion

So far, the PML tumor suppressor protein, which forms PML-NBs, has been implicated in host antiviral defenses [6,7]. In fact, PML is induced by interferon after viral infection and suppresses some viral replication [6,7]. In contrast, PML-NBs are often disrupted or sequestered in the cytoplasm by infection with several DNA or RNA viruses to protect from the antiviral function of PML [6,7,23]. In case of HCV, Herzer et al. recently reported that the HCV core protein colocalizes with PML in PML-NBs and abrogates the PML function through interaction with PML isoform IV by over-expression studies [5]. However, we did not observe such colocalization of HCV core with PML and HCV did not affect the formation of PML-NBs in response to HCV-JFH1 infection (Fig. 3E). Interestingly, Watashi et al., previously demonstrated the HCV core modulates the retinoid signaling pathway through sequestration of

Sp110b, PML-related potent transcriptional corepressor of retinoic acid receptor, in the cytoplasm from nucleus [25].

In contrast, we have demonstrated that PML is required for infectious HCV production (Fig. 1). However, the molecular mechanism(s) how PML regulates HCV production yet remains unclear. At least, PML seems to be unrelated to the HCV RNA replication (Fig. 2). In this regard, several host factors including apolipoprotein E, components of ESCRT system, and PA28γ have been implicated in infectious HCV production [13,26,27]. Indeed, PA28γ, a proteasome activator, interacts with HCV core and affects nuclear retention and stability of the core protein. Importantly, PA28γ participates in the propagation of infectious HCV by regulation of degradation of the core protein [27]. Intriguingly, Zannini reported that PA28γ interacts with PML and Chk2 and affects PML-NBs number [28]. Accordingly, we demonstrated that ATM and Chk2, which phosphorylates PML and regulates the PML function, are involved in HCV life cycle [11]. In addition, other PML-related proteins such as INI1 and DDX5 seem to be involved in HCV production (Fig. 4). Indeed, INI1, also known as hSNF5, is incorporated into HIV-1 virion and is required for efficient HIV-1 production [29]. On the other hand, cytoplasmic PML may be involved in HCV production, since endoplasmic reticulum (ER) and lipid droplets are important cytoplasmic organelle for the HCV life cycle. In this regard, Giorgi et al. recently reported that cytoplasmic PML specifically enriches at ER [30], suggesting that cytoplasmic PML may be associated with HCV production. Altogether, the PML pathway seems to be involved in infectious HCV production.

Acknowledgments

We thank Drs. Didier Trono, Reuven Agami, Richard Iggo, Toshio Kitamura, Kenichi Abe and Apath LLC for the VSV-G-pseudotyped HIV-1-based vector system pCMVΔR8.91, pMDG2, pSUPER, pRDI292, Plat-E cells, pJRN/3-5B and pJFH1. We also thank Mr. Takashi Nakamura and Ms. Keiko Takeshita for their technical assistance. This work was supported by a Grant-in-Aid for Scientific Research (C) from the Japan Society for the Promotion of Science (JSPS), by a Grant-in-Aid for Research on Hepatitis from the Ministry of Health, Labor, and Welfare of Japan, and by the Viral Hepatitis Research Foundation of Japan. M. K. was supported by a Research Fellowship from JSPS for Young Scientists.

References

[1] N. Kato, Molecular virology of hepatitis C virus, Acta. Med. Okayama 55 (2001) 133–159.
[2] N. Kato, M. Hijikata, Y. Ootsuyama, et al., Molecular cloning of the human hepatitis C virus genome from Japanese patients with non-A, non-B hepatitis, Proc. Natl. Acad. Sci. USA 87 (1990) 9524–9528.
[3] Y. Miyanari, K. Atsuzawa, N. Usuda, et al., The lipid droplet is an important organelle for hepatitis C virus production, Nat. Cell Biol. 9 (2007) 1089–1097.
[4] D.R. McGivern, S.M. Lemon, Tumor suppressors, chromosomal instability, and hepatitis C virus-associated liver cancer, Annu. Rev. Pathol.: Mech. Dis. 4 (2009) 399–415.
[5] K. Herzer, S. Weyer, P.H. Krammer, et al., Hepatitis C virus core protein inhibits tumor suppressor protein promyelocytic leukemia function in human hepatoma cells, Cancer Res. 65 (2005) 10830–10837.
[6] R.D. Everett, M.K. Chelbi-Alix, PML and PML nuclear bodies: implications in antiviral defence, Biochimie 89 (2007) 819–830.
[7] E.L. Reineke, H.Y. Kao, Targeting promyelocytic leukemia protein: a means to regulating PML nuclear bodies, Intl. J. Biol. Sci. 5 (2009) 366–376.
[8] M. Kuroki, Y. Ariumi, M. Ikeda, et al., Arsenic trioxide inhibits hepatitis C virus RNA replication through modulation of the glutathione redox system and oxidative stress, J. Virol. 83 (2009) 2338–2348.
[9] T. Wakita, T. Pietschmann, T. Kato, et al., Production of infectious hepatitis C virus in tissue culture from a cloned viral genome, Nat. Med. 11 (2005) 791–796.
[10] Y. Ariumi, M. Kuroki, K. Abe, et al., DDX3 DEAD-box RNA helicase is required for hepatitis C virus RNA replication, J. Virol. 81 (2007) 13922–13926.
[11] Y. Ariumi, M. Kuroki, H. Dansako, et al., The DNA damage sensors ataxia-telangiectasia mutated kinase and checkpoint kinase 2 are required for hepatitis C virus RNA replication, J. Virol. 82 (2008) 9639–9646.
[12] Y. Ariumi, M. Kuroki, Y. Kushima, et al., Hepatitis C virus hijacks P-body and stress granule components around lipid droplets, J. Virol. 85 (2011) 6882–6892.
[13] Y. Ariumi, M. Kuroki, M. Maki, et al., The ESCRT system is required for hepatitis C virus production, PLoS One 6 (2011) e14517.
[14] M. Ikeda, K. Abe, H. Dansako, et al., Efficient replication of a full-length hepatitis C virus genome, strain O, in cell culture, and development of a luciferase reporter system, Biochem. Biophys. Res. Co. 329 (2005) 1350–1359.
[15] T.P. Brummelkamp, R. Bernard, R. Agami, A system for stable expression of short interfering RNAs in mammalian cells, Science 296 (2002) 550–553.
[16] A.J. Bridge, S. Pebernard, A. Ducraux, et al., Induction of an interferon response by RNAi vectors in mammalian cells, Nat. Genet. 34 (2003) 263–264.
[17] Y. Ariumi, F. Serhan, P. Turelli, et al., The integrase interactor 1 (INI1) proteins facilitate Tat-mediated human immunodeficiency virus type 1 transcription, Retrovirology 3 (2006) 47.
[18] L. Naldini, U. Blömer, P. Gallay, et al., In vivo gene delivery and stable transduction of nondividing cells by a lentiviral vector, Science 272 (1996) 263–267.
[19] R. Zufferey, D. Nagy, R.J. Mandel, et al., Multiply attenuated lentiviral vector achieves efficient gene delivery in vivo, Nat. Biotechnol. 15 (1997) 871–875.
[20] B.D. Lindenbach, M.J. Evans, A.J. Syder, et al., Complete replication of hepatitis C virus in cell culture, Science 309 (2005) 623–626.
[21] K. Ishii, K. Murakami, S.S. Hmwe, et al., Trans-encapsidation of hepatitis C virus subgenomic replicon RNA with viral structure proteins, Biochem. Biophys. Res. Co. 371 (2008) 446–450.
[22] E. Steinmann, C. Brohm, S. Kallis, et al., Efficient trans-encapsidation of hepatitis C virus RNAs into infectious virus-like particles, J. Virol. 82 (2008) 7034–7046.
[23] P. Turelli, V. Doucas, E. Craig, et al., Cytoplasmic recruitment of INI1 and PML on incoming HIV preintegration complexes: interference with early steps of viral replication, Mol. Cell 7 (2001) 1245–1254.
[24] G.J. Bates, S.M. Nicol, B.J. Wilson, et al., The DEAD box protein p68: a novel transcriptional coactivator of the p53 tumor suppressor, EMBO J. 24 (2005) 543–553.
[25] K. Watashi, M. Hijikata, A. Tagawa, et al., Modulation of retinoid signaling by a cytoplasmic viral protein via sequestration of Sp110b, a potent transcriptional corepressor of retinoic acid receptor, from the nucleus, Mol. Cell. Biol. 23 (2003) 7498–7509.
[26] K.S. Chang, J. Jiang, Z. Cai, et al., Human apolipoprotein E is required for infectivity and production of hepatitis C virus in cell culture, J. Virol. 81 (2007) 13783–13793.
[27] K. Moriishi, I. Shoji, Y. Mori, et al., Involvement of PA28γ in the propagation of hepatitis C virus, Hepatology 52 (2010) 411–420.
[28] L. Zannini, G. Buscemi, E. Fontanella, et al., REGγ/PA28γ proteasome activator interacts with PML and Chk2 and affects PML nuclear bodies number, Cell Cycle 8 (2009) 2399–2407.
[29] E. Yung, M. Sorin, A. Pal, et al., Inhibition of HIV-1 virion production by a transdominant mutant of integrase interactor 1, Nat. Med. 7 (2001) 920–926.
[30] C. Giorgi, K. Ito, H.K. Lin, et al., PML regulates apoptosis at endoplasmic reticulum by modulating calcium release, Science 330 (2010) 1247–1251.

Hepatitis C virus NS4B targets lipid droplets through hydrophobic residues in the amphipathic helices[S]

Torahiko Tanaka,[1,*] Kazumichi Kuroda,[†] Masanori Ikeda,[§] Takaji Wakita,[**] Nobuyuki Kato,[§] and Makoto Makishima[*]

Division of Biochemistry, Department of Biomedical Sciences* and Division of Microbiology, Department of Pathology and Microbiology,[†] Nihon University School of Medicine, Tokyo 173-8610, Japan; Department of Tumor Virology,[§] Okayama University Graduate School of Medicine, Dentistry, and Pharmaceutical Sciences, Okayama 700-8558, Japan; and Department of Virology II,[**] National Institute of Infectious Diseases, Tokyo 162-8649, Japan

Abstract Lipid droplets (LD) are dynamic storage organelles that are involved in lipid homeostasis. Hepatitis C virus (HCV) is closely associated with LDs. HCV Core and nonstructural (NS) proteins colocalize with LDs and presumably are involved in virion formation at that site. We demonstrated that HCV NS4B, an integral membrane protein in endoplasmic reticulum (ER), strongly targeted LDs. Confocal imaging studies showed that NS4B localized at the margins of LDs. Biochemical fractionation of HCV-replicating cells suggested that NS4B existed in membranes associated with LDs rather than on the LD surface membrane itself. The N- and C-terminal cytosolic domains of NS4B showed targeting of LDs, with the former being much stronger. In both domains, activity was present in the region containing an amphipathic α-helix, in which 10 hydrophobic residues were identified as putative determinants for targeting LDs. JFH1 mutants with alanine substitutions for the hydrophobic residues were defective for virus replication. W43A mutant with a single alanine substitution showed loss of association of NS4B with LDs and severely reduced release of infectious virions compared with wild-type JFH1. NS4B plays a crucial role in virus replication at the site of virion formation, namely, the microenvironment associated with LDs.—Tanaka, T., K. Kuroda, M. Ikeda, T. Wakita, N. Kato, and M. Makishima. **Hepatitis C virus NS4B targets lipid droplets through hydrophobic residues in the amphipathic helices.** ***J. Lipid Res.*** **2013.** 54: **881–892.**

Supplementary key words alanine substitution • confocal imaging • JFH1 • RNA transfection

Cellular lipid droplets (LD) are dynamic organelles connecting storage, metabolism, and dynamics of lipids in eukaryotic cells (1–3). LDs consist of core neutral lipids, mainly triglycerides and cholesteryl esters, and the surrounding phospholipid monolayer. The lipids stored in LDs are used for various cellular events, such as metabolism as an energy source, membrane synthesis, steroid and eicosanoid synthesis, lipoprotein formation, and protein modification. LDs are thought to be generated from endoplasmic reticulum (ER) and move in a microtubule-dependent, bidirectional manner, interacting with other organelles, such as ER, mitochondria, and peroxisomes.

Recently, a close association between LDs and hepatitis C virus (HCV) was revealed (4). HCV infects about 150 million to 200 million people worldwide, and chronic infection is associated with liver steatosis, cirrhosis, and hepatocellular carcinoma. HCV is a positive- and single-stranded RNA virus with about 9,600 nucleotides of genome (5), which codes 10 HCV proteins: Core, envelope 1 (E1), envelope 2 (E2), p7, nonstructural protein (NS)2, NS3, NS4A, NS4B, NS5A, and NS5B. All of these proteins are essential for replication of HCV. Both the 5′ and 3′ untranslated regions (UTR) of the genome are also essential for viral replication: the 5′ UTR has an internal ribosome entry site (6), and the 3′ UTR contains a highly conserved structure, the 3′ X (7, 8). The infectious viral particles were found to contain the VLDL components, such as triglycerides, cholesterol, and apoB and E, and are therefore called "lipoviroparticles" (9–12). HCV infects cells by utilizing the LDL receptor and scavenger receptor B1 in addition to other receptor molecules, such as CD81, claudin 1, and occludin (13). Through the life cycle of HCV, namely, from viral entry to virion release, cellular lipids

This work was supported by the Strategic Research Base Development Program for Private Universities subsidized by the Ministry of Education, Culture, Sports, Science and Technology, Japan (since 2010); by Nihon University Multidisciplinary Research Grant (2010–2011); and by grants-in-aid for research on hepatitis from the Ministry of Health, Labour, and Welfare of Japan.

Manuscript received 20 March 2012 and in revised form 10 January 2013.

Published, JLR Papers in Press, January 12, 2013
DOI 10.1194/jlr.M026443

Abbreviations: ADRP, adipose differentiation-related protein; EGFP, enhanced green fluorescent protein; ER, endoplasmic reticulum; GST, glutathione S-transferase; HCV, hepatitis C virus; LD, lipid droplet; NS, nonstructural (protein); PNS, post-nuclear supernatant; PVDF, polyvinylidene difluoride; UTR, untranslated region.

[1] To whom correspondence should be addressed.
e-mail: tanaka.torahiko@nihon-u.ac.jp

[S] The online version of this article (available at http://www.jlr.org) contains supplementary data in the form of six figures and four tables.

and lipid metabolism, especially in lipoproteins, play important roles (10–12). HCV modulates cellular lipid metabolism to facilitate its replication: for example, HCV upregulates lipogenesis, resulting in accumulation of triglycerides in the increased mass of LDs. Clinically, liver steatosis is found in about half of chronic HCV patients. Liver steatosis occurs also in transgenic mice harboring the HCV Core protein (14). Inhibition of microsomal triglyceride transfer protein activity and VLDL secretion by HCV protein(s) is also an important mechanism of the lipid accumulation in hepatocytes (11). Several studies have shown that many HCV-derived components, such as Core (15) and NS proteins [NS2 (16), NS3, NS4A, NS4B, NS5A (17), and NS5B] and HCV RNAs, also localize at sites close to LDs (4). Core and NS5A are thought to mediate association of these HCV components with LDs (4); however, the molecular mechanisms by which NS proteins associate with LDs remain unclear. Ultrastructural studies showed accumulation of virion-like structures around LDs (18). Although several cellular and viral proteins localize on the LD membrane, consensus signals for LD targeting are not defined (1). Recent reports have shown that LD-targeting activity resides in amphipathic helices (19–23) or in hydrophobic regions (24–26).

Here, we present evidence that HCV NS4B strongly targets LDs. NS4B is a 261-amino-acid, multifunctional protein consisting of N- and C- terminal cytosolic domains and a central membrane domain harboring at least four transmembrane helices (27). NS4B is an integral membrane protein in ER (28) that can induce alteration of the membrane structure to form a membranous web (29), in which HCV RNA replication is thought to occur (30–32). We provide evidence to suggest how ER-resident protein NS4B can interact with LDs. Imaging studies, including a series of mutation analyses, revealed the regions responsible for LD targeting of NS4B. The hydrophobic amino acid residues in amphipathic α-helices are critical for LD targeting. The JFH1 (33) mutant harboring alanine substitutions for the hydrophobic residues of NS4B was defective for virus replication. In a single alanine substitution mutant, W43A, we observed that loss of LD targeting of NS4B caused a severe defect in virus replication. Our results strongly suggest that NS4B functions at sites close to LDs, which is critical for replication of HCV.

MATERIALS AND METHODS

Cell culture system

Oc cells (34) and OR6 HCV-RNA-replicating cells (35) were cultured in collagen (type I)-coated dishes (Iwaki, Chiba, Japan) with DMEM (Sigma) supplemented with 10% FBS, penicillin, and streptomycin.

Antibodies

The antibodies used in this study were those against Core (CP11; MBL, Nagoya, Japan), NS3 (R212), NS4B (52-1, detection for HCV-O NS4B), NS4AB (RR12, detection for JFH1 NS4B), NS5A (8926; BioAcademia, Osaka, Japan), NS5B (NS5B-6, BioAcademia), adipose differentiation-related protein (ADRP; Abcam), FLAG (Sigma), myc-tag (MBL), mCherry (Clontech), glyceraldehyde-3-phosphate dehydrogenase (GAPDH; Millipore), and calnexin (BD Transduction Laboratories). The anti-NS3 (R212), anti-NS4B (52-1), and anti-NS4AB (RR12) antibodies were gifts from Dr. M. Kohara (Tokyo Metropolitan Institute of Medical Science, Japan). Rabbit polyclonal antibodies specific to JFH1 NS3, NS5A, and NS5B were raised against bacterially expressed glutathione S-transferase (GST)-NS3 (amino acids 165–631), GST-NS5A (amino acids 25–466), and GST-NS5B (amino acids 1–570), respectively. Alexa-Fluor-555-conjugated anti-rabbit IgG (Invitrogen), Alexa-Fluor-568-conjugated anti-mouse IgG (Invitrogen), and rhodamine-conjugated anti-mouse IgG (Cappel) antibodies were also used.

Expression plasmids

HCV sequences for expression experiments (NS4B, NS5A and Core) were derived from type 1b HCV strain O [HCV-O, DDBJ/EMBL/GenBank accession number AB191333 (34)]. The HCV fragment was amplified by PCR using the restriction-site-tagged primers with an appropriate template plasmid that contained the desired HCV sequence. To create fusion constructs with fluorescent protein, the *Bgl*II-*Eco*RI-digested PCR fragment was ligated with *Bgl*II-*Eco*RI-digested pmCherry-C1 or pEGFP-C1 vector (Clontech). In another case, the *Nhe*I-*Hin*dIII-digested PCR fragment was ligated with *Nhe*I-*Hin*dIII-digested pcDNA3.1(+) vector (Invitrogen) to create expression constructs. To create a mutant fragment, primers that had desired mutated sequences were used for PCR, and usually two appropriate PCR fragments, namely, "-N" and "-C," were connected by overlapping PCR. Sequences of the primers and their usage, and which fragment the primer sets amplified, are described in supplementary Tables I and II, respectively. pDsRed2-ER, which expressed an ER marker protein, was obtained from Clontech. For construction of enhanced green fluorescent protein (EGFP)-ADRP and Cherry-ADRP, ADRP cDNA was synthesized from Superscript III (Invitrogen) with a primer 5′-CCACAGCATGCACTAGTGAT-3′ from total RNAs prepared from Oc cells with Trizol reagent (Life Technologies) according to the manufacturer's protocol. The ADRP fragment was amplified using the restriction-site-tagged primers 5′-TTTAGATCTATGGCATCCGTTGCAGTTGA-3′ and 5′-TTTGAATTCTTAATGAGTTTTATGCTCAGATCGC-3′, digested with *Bgl*II and *Eco*RI, and ligated with the *Bgl*II-*Eco*RI-digested pmCherry-C1 or pEGFP-C1 vector.

Transient expression experiment

Oc cells (10^5 cells/well) were seeded on a glass-based, 24-well culture plate (EZView, Iwaki), and after being cultured for 16 h, the cells were transfected with expression plasmids with the aid of Lipofectamine 2000 (Invitrogen) according to the manufacturer's protocol. Usually, 1.6 μg plasmid was used for each well with 1:2.5–3 ratio to the lipofection reagent. When two kinds of plasmids were cotransfected into cells, 1.0–1.6 μg of the plasmid was used.

Immunofluorescence

After 24 h transfection, the cells were fixed with 4% paraformaldehyde for 15 min, permeabilized with 0.01% digitonin for 30 min, and stained with Bodipy 493/503 as described previously (36). When antigens were visualized by indirect immunofluorescence, the fixed permeabilized cells were blocked with 1% BSA in TBS (20 mM Tris-HCl, 0.15 M NaCl, pH 7.4) and reacted with an appropriate dilution of primary antibody in 1% BSA-TBS for 1 h at room temperature. After three washes with TBS, the cells were incubated with an Alexa-Fluor-dye-conjugated (Invitrogen) or rhodamine-conjugated (Cappel) secondary antibody with 1,000-fold dilution in 1% BSA-TBS for 30 min. Cell nuclei were stained with Hoechst 33342 for 20 min (nuclei were stained in most of the

experiments but not always shown in the figures). The fluorescent images were collected by confocal laser scanning microscope FV1000 (Olympus, Tokyo, Japan) in a sequential scanning mode.

Immunoblotting

Proteins were resolved on 8 or 12% SDS-PAGE and transferred to polyvinylidene difluoride (PVDF) membranes (GE Healthcare). The membranes were rinsed in water and then soaked in TBS-0.1% Tween 20 (TBST) for 30 min to enhance detection sensitivity (37). The membranes were again rinsed in water and blocked with PVDF Blocking Reagent (Toyobo, Osaka, Japan) for 1 h at room temperature. The membranes were reacted with an appropriate dilution of primary antibody in Can Get Signal Immunoreaction Enhancer Solution 1 (Toyobo) for 1 h at room temperature. After washing with TBST (five times for 10 min each), the membranes were reacted with an appropriate dilution of horseradish-peroxidase-conjugated secondary antibody in Can Get Signal Immunoreaction Enhancer Solution 2 (Toyobo) for 30 min at room temperature. After washing with TBST (five times for 10 min each), the blots were visualized by an ECL Plus immunoblot detection system (GE Healthcare).

Construction of JFH1 mutant

We generated JFH1 (33) (DDBJ/EMBL/GenBank accession number AB047639) mutant constructs that contained alanine substitutions for hydrophobic residues in the NS4B region as follows: 4Bmtmt, W43A, V46A, W50A, F57A, I61A, L64A, I242A, L246A, L249A, and I253A; 4Bmt0, W43A, V46A, W50A, F57A, I61A, and L64A; 4Bmt1, W43A, V46A, and W50A; 4Bmt2, F57A, I61A, and L64A; and 4Bmt3, I242A, L246A, L249A, and I253A. Mutants harboring single alanine substitutions, W43A, V46A and W50A, were also created. To create a mutant fragment, primers with the desired mutated sequences were used for PCR, and two or three appropriate PCR fragments ("-N" and "-C"; or "-N1," "-N2," and "-C") were connected by overlapping PCR. The resultant mutant fragment was digested with *Nsi*I and *Rsr*II and ligated with *Nsi*I-*Rsr*II-digested pJFH1 (33). Sequences of the primers and their usage and which fragment the primer sets amplified are described in supplementary Tables III and IV, respectively.

In vitro transcription and electroporation of viral RNA into Oc cells

pJFH1 and its mutant plasmids were linearized with *Xba*I followed by treatment with mung bean nuclease (Toyobo) according to the manufacturer's protocol. RNA was transcribed in vitro from the linearized constructs using MEGAscript T7 kit (Ambion) and purified with MEGAclear kit (Ambion) according to the instruction manual. RNA integrity was checked by agarose gel electrophoresis. Prior to electroporation, Oc cells were trypsinized and resuspended in complete DMEM. The cells were washed twice with PBS and resuspended in buffer R (Invitrogen) at a concentration of 10^7 cells/ml. JFH1 and mutant RNA was introduced into the Oc cells using the NEON transfection system (Invitrogen) according to the instruction manual as follows. For titration of virus production, 0.5 μg RNA was introduced into 10^5 cells in a 10 μl tip supplied by the manufacturer with two pulses of 30 ms at 1,150 V. Usually, four shots of the electroporated cells (4×10^5 cells) are pooled in 4 ml prewarmed DMEM supplemented with 10% FBS and seeded into 12-well plates (1 ml for each well). For preparation of LDs, 5 μg RNA was introduced into 10^6 cells in a 100 μl tip supplied by the manufacturer, with two pulses of 30 ms at 1,150 V. Three shots of the electroporated cells (3×10^6 cells) were pooled in 30 ml prewarmed DMEM supplemented with 10% FBS and seeded into dishes with a diameter of 10 cm (10 ml each). At 48 h posttransfection, LDs were prepared as described below.

Cell fractionation by step-wise sucrose density gradient

OR6 cells were fractionated in sucrose density gradient as described previously (38) with minor modifications. Twelve hours before preparation, 100 μM oleate was added to the culture medium. Cells (2×10^6 to 3×10^6 cells) were homogenized in 0.5 ml buffer A [10 mM tricine, 3 mM EDTA, and Complete Protease Inhibitor Cocktail (Roche), pH 7.4] containing 0.25 M sucrose with 30 strokes of a glass Dounce homogenizer using a tight-fitting pestle. The lysate was centrifuged for 10 min at 1,000 *g* at 4°C. The sucrose concentration of the postnuclear supernatant (PNS) was adjusted to 26% by adding buffer A containing 60% sucrose. In a 5 ml ultracentrifuge tube (5PA; Hitachi Koki, Tokyo, Japan), 0.34 ml buffer A containing 51% sucrose and 0.75 ml buffer A containing 43% and 35% sucrose were layered. Subsequently, 0.63 ml 26% sucrose-PNS was layered on top of this. Following this, 0.75 ml buffer A containing 18% and 10% sucrose was layered sequentially onto the PNS fraction. Finally, 0.97 ml of buffer A containing 2% sucrose was loaded on top. The step-wise gradient was centrifuged at 32,000 rpm, at 4°C for 90 min using an S52ST rotor (Hitachi Koki). Following centrifugation, the samples (0.5 ml each) were collected from the bottom.

Preparation of LDs

LDs were prepared as described previously (4) with minor modifications. Twelve hours before preparation, 100 μM oleate was added to the culture medium. Samples and buffers were handled on ice or at 4°C through the procedures below. Cells (~3×10^6 OR6 or Oc cells transfected with JFH1 or mutant RNA) were pelleted by centrifugation at 3000 rpm for 5 min at 4°C. The pellet was resuspended in 1.2 ml hypotonic buffer (50 mM HEPES, 1 mM EDTA, 2 mM $MgCl_2$, and Complete Protease Inhibitor Cocktail, pH 7.4) and incubated for 10 min. The suspension was homogenized with 30 strokes of a glass Dounce homogenizer using a tight-fitting pestle, followed by addition of 120 μl 10× sucrose buffer [0.2 M HEPES, 1.2 M potassium acetate, 40 mM $Mg(oAc)_2$, and 50 mM DTT, pH 7.4]. The nuclei were removed by centrifugation at 2,000 rpm for 10 min at 4°C. The supernatant was collected and centrifuged at 16,000 *g* for 10 min at 4°C. The supernatant (S16, 1.25 ml) was mixed with 1.25 ml 1.04 M sucrose in isotonic buffer (50 mM HEPES, 100 mM KCl, 2 mM $MgCl_2$, and Complete Protease Inhibitor Cocktail). The solution was set at the bottom of 5 ml 5PA ultracentrifuge tubes, and 2.5 ml isotonic buffer was loaded onto the sucrose mixture. The gradient was centrifuged at 100,000 *g* in an S52ST rotor for 45 min at 4°C. After centrifugation, the LD fraction on the top of the gradient solution was collected as the first LD fraction (LD1). After 0.1 ml of the fraction was removed for analysis, the volume of the LD1 fraction was then adjusted to 1.25 ml with isotonic buffer and the fraction was mixed with 1.25 ml isotonic buffer containing 1.04 M sucrose. The fraction was set at the bottom of the ultracentrifuge tube and centrifuged again at 100,000 *g* as described above. The LD fraction on the top of the gradient solution was collected as the second LD fraction (LD2).

Titration of HCV infection

Culture supernatant of RNA-transfected cells was filtrated (0.45 μm pore filter) and assayed for infectivity titer by the end-point dilution method. Before 16 h inoculation, Oc cells were seeded into 96-well plates at a density of 8×10^3/well. Samples were serially diluted 10-fold in complete growth medium, and 20 μl (when necessary, 100 μl) was inoculated into Oc cells in each well in duplicate. After three days of incubation, the cells were

immunostained by anti-Core antibody (CP11). Positive foci were counted, and the infectivity titer was calculated from the average number of foci counted in the last and second-to-last wells of the dilution series that still contained positive foci. The virus titer was expressed as focus-forming units per milliliter of supernatant.

RESULTS

The intrinsic localization of NS4B to LDs

To clarify whether NS4B associated with LDs by itself and the mechanisms of LD targeting by NS4B, we performed fluorescent imaging using confocal microscopy (**Fig. 1** and supplementary Fig. I). NS4B was fused with mCherry or EGFP, and subcellular localization of the fusion proteins was observed simultaneously with that of LDs in Oc cells. LDs were visualized by Bodipy 493/503. We confirmed that the native forms of mCherry or EGFP, found in both cytosol and the nucleus, showed no colocalization with LDs (supplementary Fig. I-A). When the full-length NS4B was fused with the color proteins (Cherry-4B1–261 and EGFP-4B1–262), a major portion of NS4B showed a membranous, reticular pattern of localization in both cases, suggesting the localization to ER. Upon coexpression with an ER marker construct pDsRed2-ER (DsRed-ER), which contained the ER-targeting sequence of calreticulin and the ER retention signal KDEL, localization of NS4B was consistent with that of the ER marker (supplementary Fig. I-A). This suggested that the full-length NS4B resided in ER membrane as previously reported (28, 39). However, we found a small level of ring-shaped localization of NS4B surrounding the green circular fluorescence of Bodipy, which may correspond to the margin of LDs (Fig. 1A and supplementary Fig. I-B). This ring-shape localization pattern merged with that obtained with anti-ADRP antibody (data not shown), suggesting that NS4B localized to the surface of LDs (LD membrane itself or ER membranes associated with LDs). To confirm the colocalization of NS4B with ADRP, we made fusion constructs of ADRP with color fluorescent proteins and coexpressed them with NS4B (Fig. 1B). The fusion constructs of ADRP (Cherry-ADRP and EGFP-ADRP) showed clear ring-shape localization, and the images of Cherry-ADRP and EGFP-ADRP were completely merged, indicating their localization to the LD membranes (Fig. 1B). When Cherry-4B1–261 was coexpressed with EGFP-ADRP, a portion of Cherry-4B1–261 showed ring-shape localization that was consistent with that of EGFP-ADRP, suggesting colocalization of the fusion proteins (Fig. 1B and supplementary Fig. I-C). Thus, a portion of expressed NS4B was thought to localize on the surface of LDs. To represent the degree of LD targeting for each

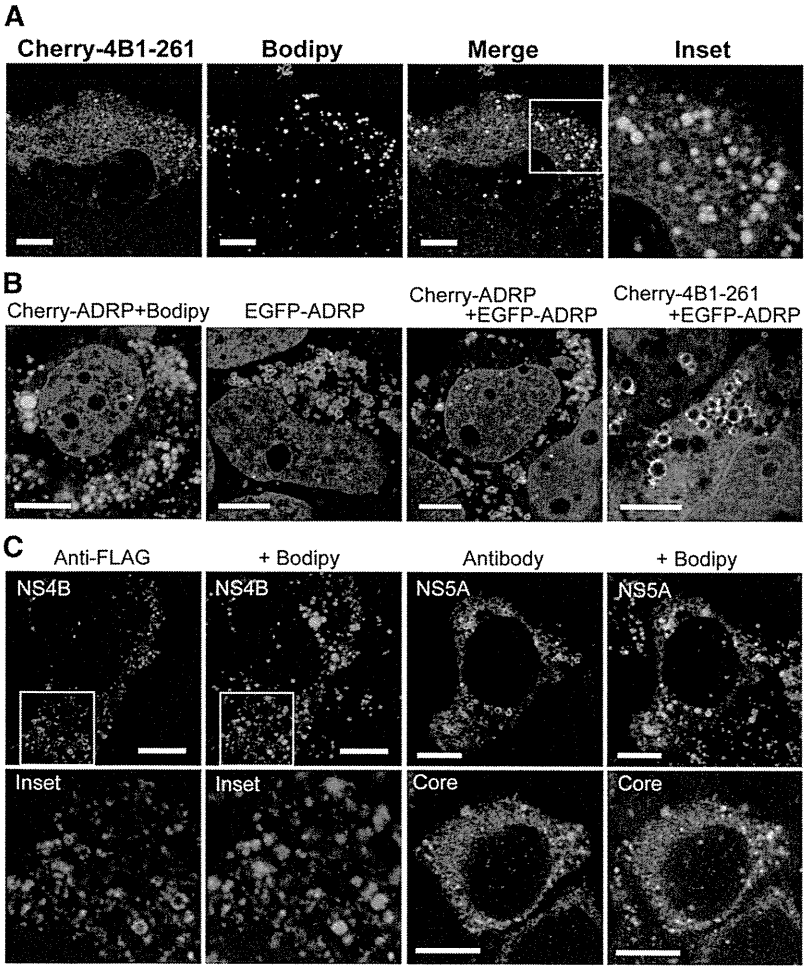

Fig. 1. Full-length NS4B localizes to LDs. (A) Localization of Cherry-4B1–261. Oc cells were transfected with Cherry-4B1–261 for 24 h followed by staining with Bodipy493/503. (A, inset) magnified image. Scale bars, 10 μm. (B) Colocalization of Cherry-4B1–262 with ADRP. From left, Cherry-ADRP, EGFP-ADRP, Cherry-ADRP with EGFP-ADRP (cotransfection), and Cherry-4B1–261 with EGFP-ADRP (cotransfection) was transfected into Oc cells. Scale bars, 10 μm. (C) Localization of NS4B, NS5A, and Core protein. Oc cells were transfected with pcDNA-4B1–261-FLAG (left), pcDNA-5A-myc (right, top), or pcDNA-CORE (right, bottom) for 24 h. After fixation, the antigens were visualized with anti-FLAG (NS4B), anti-Myc (NS5A), or anti-Core antibodies and Alexa-Fluor-dye-labeled secondary antibodies. Scale bars, 10 μm. Inset, magnified image.

construct, we categorized the NS4B-expressing cells (for at least 50 transfectants) into the following four categories: exclusive or dominant localization of the protein to LDs in the observed section (category I); apparent (but not dominant) localization to LDs (category II); slight localization to LDs (with 1–5 rings surrounding LDs seen in the section, category III); and no localization to LDs (category IV). For Cherry-4B1–261 transfectant, about 4 and 15% of the cells were classified into categories I and II, respectively (the results of the count are described in **Table 1**). Thus, NS4B colocalized with LDs in about 20% of cells.

We next expressed full-length NS4B fused with an epitope tag FLAG (amino acid sequence, DYKDDDDK) (pcDNA4B1–261-FLAG) and detected it using an anti-FLAG antibody (this is because we could not obtain antibodies that detected NS4B in HCV-O via immunofluorescence). In most cases, the stain showed differently sized dots, but no clear reticular pattern was obtained. However, we also found that, in some cells, the small dots of NS4B surrounded LDs, suggesting LD localization of FLAG-tagged NS4B (Fig. 1C). Thus, NS4B localizes to LDs by itself. A similar pattern of LD localization was observed for HCV NS5A [tagged with myc (EQKLISEEDL) at the C terminus] and Core, which are known to associate with the LD surface (Fig. 1C). We also found that NS5AΔ1–30, which lacks the N-terminal amphipathic α-helix (amino acids 1–30), did not localize to LDs (data not shown). We conclude that NS4B has an intrinsic activity to target the surface of LDs.

Subcellular distribution of NS4B in OR6 cells

We investigated whether intact NS4B targets LDs in the presence of other HCV proteins. We could not obtain antibodies applicable to immunofluorescent study for HCV-O; therefore, we adopted a biochemical approach. Subcellular fractionation of OR6 HCV-RNA-replicating cells was performed and distribution of HCV antigens was examined by immunoblotting. In OR6 cells, genome-length RNA of HCV-O (fused with *Renilla* luciferase gene for monitoring of HCV genome replication) was stably replicated; hence, intact functional HCV antigens were expressed in the cells. Distributions of cellular and HCV antigens in fractions obtained from OR6 cells by discontinuous sucrose density gradient (38) are shown in **Fig. 2** (left). ADRP was detected most abundantly in the top fraction (fraction 10) followed by fraction 9, suggesting that LDs were enriched in fraction 10 and partly in fraction 9. Calnexin, a marker protein of ER, was found mostly concentrated in fraction 2, showing that a major portion of ER was fractionated into fraction 2. A small portion of calnexin was also enriched in fraction 9 (and 10), suggesting that this fraction contained ER membranes associated with LDs. HCV antigens (Core, NS3, NS4B, NS5A, and NS5B) were detected most abundantly in fraction 2, suggesting that these HCV antigens were associated with ER membranes. However, a small portion of HCV antigens, especially Core, NS4B and NS5A, were clearly detected in fractions 10 and 9. This suggested that a substantial amount of HCV antigens, including NS4B, were present in LD-associated ER membranes or in the LD membrane itself in OR6 cells.

We also prepared LDs from OR6 cells using sucrose density gradient fractionation (by two rounds of discontinuous sucrose gradient ultracentrifugation) as previously described (4) (Fig. 2, right). LD1 was a crude LD preparation after the first ultracentrifugation, and LD2 was the final LD preparation from the second ultracentrifugation. To evaluate the enrichment of antigens to LDs, the amount of each fraction used for immunoblotting was adjusted to give approximately equal signal intensities for ADRP. LD1 seemed to contain a small amount of ER proteins, presumably LD-associated, because a small amount of calnexin was detected in LD1. A small amount of NS4B was detected in LD1 (and a small amount in LD2 with a long chemiluminescence lifetime; data not shown). NS5A was clearly detected in LD1, and a small amount in LD2 as expected. However, Core protein was not detected in either LD preparation, even with longer exposure.

TABLE 1. LD-targeting activity of various NS4B constructs

	Category (% Cells)			
Construct	I	II	III	IV
Cherry-4B1–261[a]	3.7 ± 1.5	15 ± 7	11 ± 4	71 ± 9
Cherry-4B1–73[a]	71 ± 12	29 ± 12	0	0
Cherry-4B74–191	0	0	0	100
Cherry-4B192–261[a]	14 ± 7	34 ± 5	22 ± 9	30 ± 8
Cherry-4B1–49	0	0	0	100
Cherry-4B26–73	15	45	21	19
Cherry-4B1–25	0	0	0	100
Cherry-4B26–49	0	0	0	100
Cherry-4B50–73	0	2	21	77
Cherry-4B192–239	0	0	2	98
Cherry-4B218–261	0	0	10	90
Cherry-4B192–217	0	0	0	100
Cherry-4B218–239	0	0	0	100
Cherry-4B240–261	0	0	8	92
pcDNA-4B1–261-FLAG	0	3	5	93

The degree of LD targeting for each cell is expressed as category I, II, III, or IV. Each construct was transfected into Oc cells, and the percentages of cells with each category are shown.

[a]Results are mean ± SD from three independent experiments.

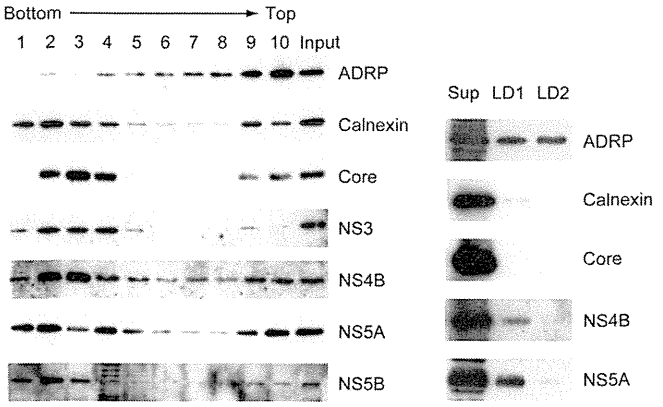

Fig. 2. Localization of HCV antigens to LDs in OR6 cells. (Left) Distribution of cellular and HCV antigens in fractions obtained by discontinuous sucrose density gradient ultracentrifugation (51, 43, 35, 26, 18, 10, and 2% sucrose from bottom to top). OR6 cells were fractionated. The 1/100 vol of each fraction (1–10) and 1/1,000 vol of original PNS (Input) were run on 12% SDS-PAGE followed by immunoblot analysis. (Right) Localization of HCV antigens to LD preparations. LDs were prepared from OR6 cells. LD1, LD preparation obtained from first ultracentrifugation; LD2, final LD preparation obtained from second ultracentrifugation; Sup (S16), supernatant after 16,000 *g* centrifugation. Fractions were analyzed by immunoblotting. The amount of each fraction applied for immunoblotting was adjusted to give approximately equal signal intensity for ADRP. The apparent molecular weights of the indicated proteins were: ADRP, 52 kDa; calnexin, 90 kDa; Core, 21 kDa; NS3, 70 kDa; NS4B, 27 kDa; NS5A, 56/58 kDa; and NS5B, 66 kDa.

NS4B of JFH1 strain targets LDs in RNA-transfected cells

HCV strain JFH1 (subtype 2a) is the first effective replication/infection system of HCV (33). When the genome-length JFH1 RNA is transfected into HuH-7 and its derivative cells, virus replication occurs in cells and infectious virion is released into the culture medium. We transfected JFH1 RNA into Oc cells and prepared and analyzed the LDs by immunoblotting (supplementary Fig. II). NS3, NS4B, NS5A, and NS5B proteins were all positive in both LD1 and LD2. NS4B was apparently enriched in LD1 as compared with the ratio of calnexin content between Sup (S16) and LD1, but it was much less abundant in LD2 than in LD1. This distribution profile suggested that NS4B was localized to LD-associated ER membranes rather than to the LD membranes themselves. Core protein was not detected in LD preparations as in those of OR6 cells; instead, it was precipitated to the bottom of the ultracentrifugation tube.

NS4B has two independent LD-targeting regions in the N- and C-terminal cytosolic domains

To determine which regions or motifs in NS4B were responsible for the targeting to LDs, various NS4B constructs of HCV-O were prepared as fusion proteins with mCherry (**Fig. 3A**). The results were similar for mCherry and EGFP constructs; therefore, we chose mCherry as a tag protein together with Bodipy 493/503 to stain LDs. We determined the activity of the N- and C-terminal cytosolic domains and the central membrane domain (Fig. 3B and Table 1). Crystal structure analysis is not yet possible for NS4B; therefore, the boundary of the N-terminal and central membrane domains was not determined. The boundary of the central and C-terminal domains has been determined from the secondary structure prediction as being between 191 and 192 (27). We tentatively defined the domains as amino acids 1–73, 74–191, and 192–261, respectively, and expressed them in Oc cells. We found that the N-terminal domain (Cherry-4B1–73) showed a strong LD localization. For Cherry-4B1–73, about 70% of the cells were counted as category I and 30% as II; therefore, in nearly all of the cells, the N-terminal domain of NS4B showed LD localization. When the membrane domain (Cherry-4B74–191) was expressed in cells, many ring-shaped localizations were seen, but they had no relation with LDs (Fig. 3B). This ring-shape structure implies that NS4B activity can alter the membrane structure of ER, forming a "membranous web" (29).

The C-terminal domain (Cherry-4B192–261) also showed LD localization, but to a lesser extent than that of the N-terminal region: ~10% of the cells were category I, and 30% were category II. To identify the detailed LD-binding region, each terminal region was further divided into three, and their localization or that of the region spanning the two parts (two thirds of the terminal domain) was determined (Fig. 3C, D and Table 1). For the N-terminal region, Cherry-4B26–73 showed significant LD targeting. Within the amino acid residues 26–73, Cherry-4B26–49 showed no activity, whereas Cherry-4B50–73 was slightly active. Although the degree of localization was much lower than that of Cherry-4B1–73, the N-terminal site for LD localization was identified in the C-terminal half (or one third) of the N-terminal domain (Table 1). Regarding the C-terminal region, Cherry-4B218–261 and Cherry-4B240–261 were slightly active, suggesting that the C-terminal site is in the C-terminal half (or one third) of the C-terminal domain, although the region had little activity by itself (Table 1). Thus, NS4B had two independent regions for targeting LDs.

Hydrophobic amino acid residues in amphipathic α-helices in NS4B are critical for LD targeting

For both the N- and C-terminal sites, an amphipathic α-helix has been identified: amino acids 40–69 for the N-terminal region, and 229–253 for the C-terminal region. Both helices are thought to mediate membrane association of NS4B (40, 41). Amphipathic helices are also known to mediate LD association (19–23); therefore, we hypothesized that the amphipathic helices, especially the hydrophobic amino acids within them, were important for LD targeting of NS4B. From helical wheel projection analysis (http://rzlab.ucr.edu/scripts/wheel/wheel.cgi, provided by D. Armstrong et al.), we noticed that 10 hydrophobic residues (43W, 46L, 50W, 57F, 61I, and 64L for the N-terminal amphipathic helix; 242I, 246L, 249L, and 253I for the C-terminal amphipathic helix) were present on the hydrophobic faces of the helices (**Fig. 4**). To establish whether these residues were involved in LD targeting, we made various alanine substitutions for the residues. The influence of mutations was evaluated by reduction of LD localization as compared with the mother constructs (Fig. 4).

When all of the six residues in the N-terminal amphipathic helix were substituted by alanine (Cherry-4B1–73mt1), the

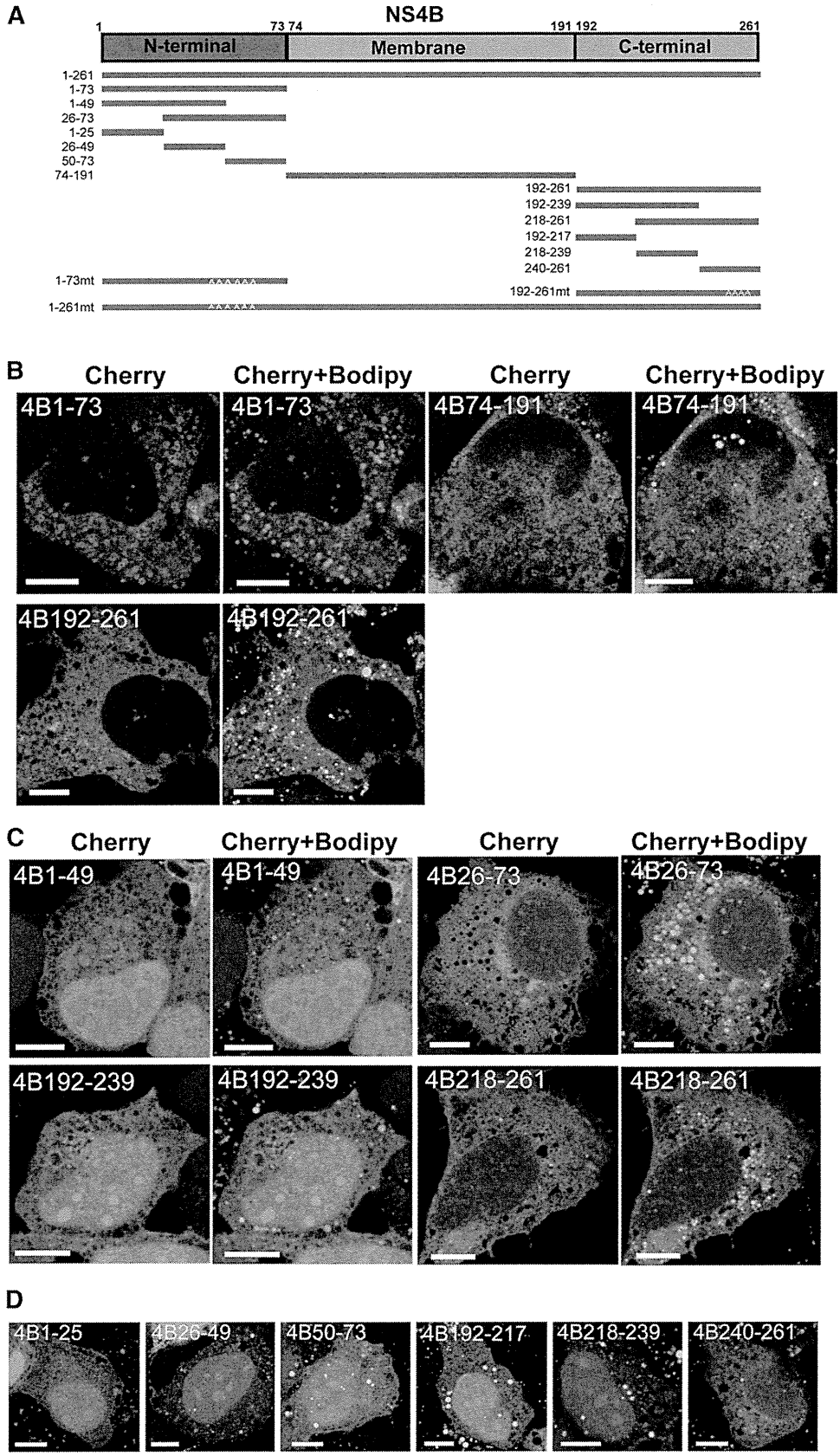

Fig. 3. Two independent target sites for LDs are present in NS4B. (A) Schematic representation of the intact and mutant NS4B. NS4B proteins were N-terminally tagged with mCherry protein. Numbers indicate the amino acid position in NS4B, and mt denotes the alanine substitution construct. (B) Localization of the N-terminal, central, and C-terminal domains of NS4B. Oc cells were transfected with Cherry-4B1–73, Cherry-4B74–191, or Cherry-4B192–261 for 24 h, and then fixed and stained with Bodipy 493/503. (C, D) Localization of the subdivided N- and C-terminal domains of NS4B. (B–D) Scale bars, 10 μm.

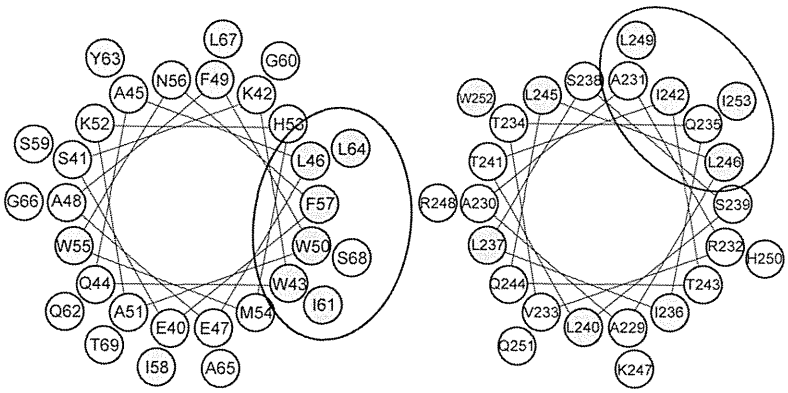

	Degree of LD targeting (Category)			
	I	II	III	IV
	(% cells)			
Cherry-4B1-73mt1 (W43A, L46A, W50A, F57A, I61A, L64A)	0	0	0	100
Cherry-4B1-73mt2 (W43A, L46A, W50A)	0	24	25	51
Cherry-4B1-73mt3 (F57A, I61A, L64A)	27	61	11	2
Cherry-4B1-73mt4 (W43A)	51	49	0	0
Cherry-4B1-73mt5 (L46A)	61	39	0	0
Cherry-4B1-73mt6 (W50A)	68	30	2	0
Cherry-4B192-261mt1 (I242A, L246A, L249A, I253A)	0	0	2	98
Cherry-4B1-261mt1 (W43A, L46A, W50A, F57A, I61A, L64A)	0	0	5	95

Fig. 4. Hydrophobic amino acid residues in amphipathic α-helices are critical for targeting LDs. (Top) Helical wheel projection analysis (http://rzlab.ucr.edu/scripts/wheel/wheel.cgi) for amphipathic α-helices in the N-terminal (left) and C-terminal (right) domains. Hydrophobic residues (W, F, Y, L, I) are shown as gray circles. The ellipse shows a putative hydrophobic face. (Bottom) Inhibition of LD-targeting activity by alanine substitutions for the hydrophobic residues. Localization to LDs was determined for each mutant, and the degree of LD targeting is presented by the percentages of cells classified into categories I–IV. Category I, expressed protein localized to LDs exclusively or dominantly; category II, expressed protein localized to LDs apparently but not dominantly (at least six ring-shape localizations surrounding LDs are seen in the section); category III, expressed protein slightly localized to LDs (1–5 ring-shape localizations surrounding LDs are seen in the section); category IV, expressed protein did not localize to LDs.

LD-targeting activity of Cherry-4B1–73 completely disappeared. As a result of a six-residue interval between 50W and 57F, the hydrophobic residues could be segregated into two clusters of three hydrophobic residues each. When the three residues of the cluster were substituted simultaneously, the influence on the LD-targeting activity was stronger by mutating the upstream cluster (Cherry-4B1–73mt2, containing W43A, L46A, and W50A) than the downstream cluster (Cherry-4B1–73mt3, containing F57A, I61A, and L64A) (Fig. 4). The single residue substitution in the upstream cluster, W43A, L46A, or W50A, did not significantly affect the LD-targeting activity of Cherry-4B1–73 (Cherry-4B1–73mt4, mt5, and mt6). The results indicated that the hydrophobic residues in the amphipathic helix were required for the LD-targeting activity in the N-terminal domain of NS4B, in which the residues in the upstream cluster (43W, 46L, and 50W) had a relatively stronger effect in a synergistic manner.

Regarding the C-terminal domain of NS4B, we made alanine substitutions for all four residues simultaneously (Cherry-4B192–261mt1, containing I242A, L246A, L249A, and I253A), because the activity of the mother Cherry-4B192–261 was relatively low (Table 1). This mutant showed no activity for LD targeting. Although the degree of contribution from each residue was not clear, these hydrophobic amino acids were considered to be critical for the LD-targeting activity of the C-terminal domain. Similarly, we made six alanine substitutions simultaneously (W43A, L46A, W50A, F57A, I61A, and L64A) in a full-length NS4B construct (Cherry-4B1–261mt1), because of the relatively low targeting activity of the mother construct Cherry-4B1–261. This alanine mutant showed no apparent activity for LD targeting, indicating that the hydrophobic residues were critical for LD targeting of full-length NS4B.

When the expression of cherry fusion proteins was checked by immunoblotting, each construct showed its predicted molecular weight, although differences in expression level were seen among the different constructs (supplementary Fig. III). Cherry-4B1–73 and its mutants showed dual bands by unknown mechanisms; however, this seemed to be unrelated to the degree of LD-targeting for each protein. It should be noted that the 10 amino acid residues described here (43W, 46L, 50W, 57F, 61I, 64L, 242I, 246L, 249L, and 253I) were highly conserved among the wide variety of subtypes of HCV, supporting their critical role in the virus life cycle (supplementary Fig. IV).

JFH1 mutants harboring alanine substitutions abolishing LD-targeting activity of NS4B are defective for replication

To clarify the importance of LD targeting of NS4B for replication of HCV, we examined JFH1 mutants that contained alanine substitutions of hydrophobic residues critical for LD targeting in the NS4B region. The 10 hydrophobic residues, 43W, 46V (L in strain O), 50W, 57F, 61I, 64L, 242I, 246L, 249L, and 253I, were divided into three clusters as described above, and mutants were created for each cluster of three or four simultaneous alanine substitutions: 4Bmt1, W43A, V46A, and W50A; 4Bmt2, F57A, I61A, and L64A; and 4Bmt3, I242A, L246A, L249A, and I253A. When the wild-type and mutant RNAs were transfected into Oc cells, wild-type JFH1 released an increasing number of infectious virions (**Fig. 5A**), whereas the cluster mutants (4Bmt1, 4Bmt2, and 4Bmt3) produced no detectable infectious virions. For all these mutants, no HCV antigens were detected by immunoblotting in transfected cells (Core, NS4B, and NS5A were tested; data not shown). The cluster mutants were defective for virus replication. We then concentrated on the first N-terminal cluster and created single alanine substitution mutants for the three hydrophobic residues, W43A, V46A, and W50A, because the cluster was considered

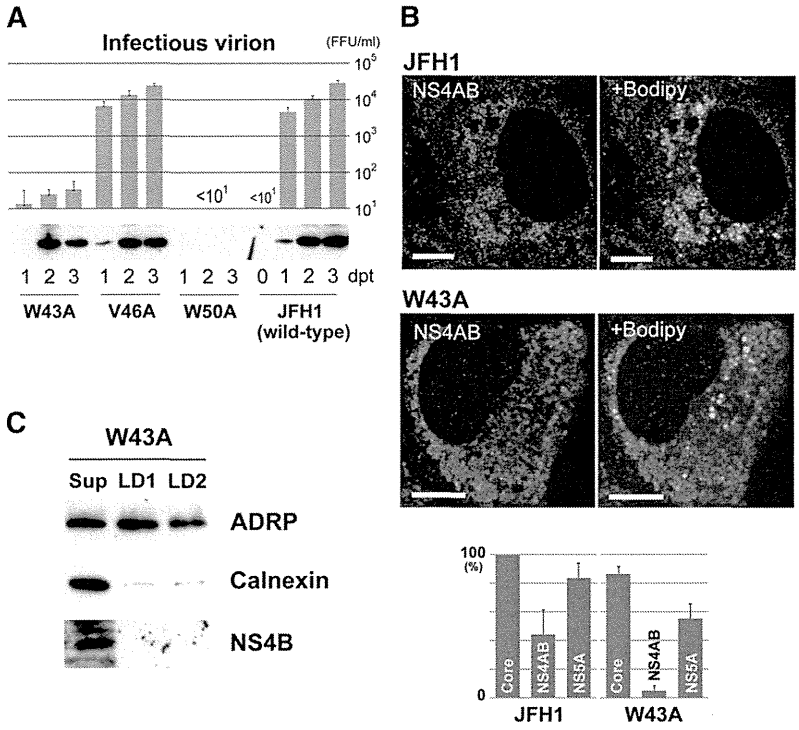

Fig. 5. JFH1 mutants harboring single alanine substitutions for hydrophobic residues of NS4B are defective for replication. (A) Effect on virus replication of alanine substitutions in NS4B region of JFH1. (Top) Titration of infectious virions released from transfectants of JFH1 or mutant RNAs. Culture supernatant of each transfectant was assayed for infectivity at the indicated days post transfection (dpt). FFU, focus forming unit. Mean values from three or four independent experiments are shown; error bars denote SD. (Bottom) Expression of NS4B in the transfectants of JFH1 or mutant RNAs. (B) Localization of HCV antigens and the changes caused by W43A mutation. (Top) Change in localization of NS4AB (NS4B and/or NS4A). Transfectants with JFH1 or W43A RNA were stained with anti-NS4AB antibody, followed by staining with Bodipy 493/503. Scale bars, 10 μm. (Bottom) Comparison of LD association for HCV antigens between W43A- and JFH1-RNA-transfected cells. The percentages of positive cells for LD association of each antigen are shown. When association was seen for at least six LDs in a section, the transfectant was counted as positive. Mean values from three independent experiments are shown; error bars denote SD. (C) Localization of NS4B to LD preparations obtained from W43A-RNA-transfected cells. LD fractions were prepared and analyzed as in Fig. 2, right.

to be most effective for LD targeting of NS4B as described above. When RNAs were transfected into Oc cells, the mutants released different numbers of infectious virions (Fig. 5A). As compared with wild-type, W43A released only 1/300 to 1/1,000 of infectious virions, and V46A released comparable amounts of virions. W50A released no detectable infectious virions. Interestingly, W43A mutant, as well as V46A, expressed comparable amounts of HCV antigens as did wild-type, as confirmed by immunoblotting (Fig. 5A). In contrast, expression of HCV antigens was negligible for W50A (only faint bands were seen with longer exposure; data not shown). Although the W50A mutant was of interest to clarify the mechanisms of the defect, further analysis was not performed.

We then analyzed by confocal microscopy LD targeting of NS4B for W43A mutant, comparing it with that of the wild-type (Fig. 5B and supplementary Fig. V). We could not obtain antibodies for immunofluorescent detection of JFH1 NS4B; therefore, we used anti-NS4AB polyclonal antibody, which reacted with both NS4A and NS4B proteins. Distributions of NS4B (and/or 4A) and other antigens were observed by confocal microscopy for transfectants of wild-type and W43A (Fig. 5B and supplementary Fig. V). For JFH1, NS4B (and/or 4A) showed a reticular staining pattern, but a considerable amount of stain was concentrated around LDs and some showed broken (incomplete) ring-shape staining surrounding the LDs. In contrast, for W43A, NS4B (and/or 4A) showed a reticular pattern or small bubble-shape staining, but the stain had no relation to the LDs. Core protein showed clear ring-shape staining at the margins of the LDs in both wild-type (supplementary Fig. V) and W43A. However, for the latter, there was a slight increase in the percentage of transfectants without ring-shape staining of Core (but with reticular pattern alone). NS5A showed the staining patterns seen for both the Core and NS4AB. For both wild-type (supplementary Fig. V) and W43A, we observed clear or broken ring-shape staining surrounding the LDs, and the stain concentrated around LDs. We also tried imaging with anti-NS3 and anti-NS5B antibodies, which were used for immunoblotting of JFH1 antigens; however, the results of staining were not informative. The percentages of transfectants positive for LD association of antigens were compared for wild-type and W43A (Fig. 5B, bottom). In W43A, LD association of NS4B (and/or 4A) was markedly decreased as compared with wild-type, whereas

that of Core and NS5A was mildly decreased. For V46A mutant, percentages of positive transfectants were 97, 28, and 79%, for Core, NS4AB, and NS5A, respectively.

Finally, we purified LD fractions from W43A transfectant and analyzed for HCV antigens by immunoblotting (Fig. 5C and supplementary Fig. VI). In contrast to LD fractions from wild-type (supplementary Fig. II), calnexin content in LD1 and LD2 was comparable, suggesting that the W43A mutation in NS4B affects membrane micro-architecture around LDs. This suggestion was supported by drastic changes in distribution of NS4B (and/or 4A) around LDs, where it seemed as if the distribution pattern of the ER membranes themselves was altered by the mutation of NS4B (Fig. 5B). In both LD1 and LD2, NS4B was not detected by immunoblotting, suggesting that NS4B harboring the W43A mutation could not interact with LDs (Fig. 5C). The other HCV antigens, NS3, NS5A, and NS5B, were detected in both LD1 and LD2 (supplementary Fig. VI). Also in W43A, the Core protein was not detected in LD fractions but in the ultracentrifugation pellet.

DISCUSSION

In the present study, we demonstrated that HCV NS4B has the ability to target LDs. In the imaging analysis using Cherry constructs, some expressed NS4B showed ring-shape structures at the margins of LDs, suggesting that NS4B was present near to LD membranes. This was confirmed by the colocalization results of NS4B with ADRP in ring-shape structures. Biochemical approaches also showed LD targeting of NS4B. It was important to establish whether LD targeting of intact NS4B protein occurred in the presence of other HCV proteins, because the HCV proteins, including NS4B, physically and functionally interact with each other during virus replication. To clarify this, we used OR6 cells in which genome-length HCV-O RNA was stably replicating, hence, functional HCV proteins were present. We found that NS4B existed in the crude LD fraction (LD1 in Fig. 2, right), suggesting that NS4B was localized to the membranes associated with LDs. Analysis of LD fractions from JFH1-RNA-transfected cells also suggested that NS4B localized to such LD-associated ER membranes rather than on the LD surface membranes themselves (supplementary Fig. II).

In cellular LD-targeting proteins, the targeting mechanism is thought to be complex and multifactorial (1). However, two major required features of amino acid sequence have been proposed: one is the amphipathic α-helix (19–23), and the other is a rather undefined hydrophobic region (24–26). Some LD-targeting proteins, such as caveolin-1 and associated with lipid droplet protein 1 (ALDI) (24, 42), showed dual localization to LDs and ER in relation with cellular lipid dynamics. One simple explanation may be that the LD-targeting sequences also have ER-targeting activity. LD biogenesis is believed to be initiated from the accumulation of lipids between the two membrane leaflets of the ER (1–3); therefore, another explanation is that proteins initially target the ER membranes and are then assorted on the emerging LD membranes by lateral diffusion with the aid of additional, yet undefined mechanisms. The latter targeting model has also been proposed for the HCV Core, in which the truncated form of the Core protein targets LDs more efficiently (22). However, this LD-assorting mechanism is unlikely for NS4B, because NS4B has at least four transmembrane helices by which the protein is integrated into the ER bilayer membrane (43). It should be noted that LDs are surrounded by lipid monolayers. Taking together the proposed sorting mechanisms of other LD-targeting proteins with the result that LD-targeting sites were present in each cytosolic domain, a likely model is that NS4B is present in the ER and that both cytosolic terminal domains interact simultaneously with the LD surface membrane through the hydrophobic residues in amphipathic helices; NS4B tethers or catches the emerging LDs on or very near to the ER (**Fig. 6**). The results from biochemical analysis of LD preparations, in which NS4B seemed to be present in LD-associated membranes rather than on the LD surface membranes themselves, support this model. To clarify whether NS4B and ADRP were present in the identical membrane structure, we also performed fluorescence recovery after photobleaching (FRAP) analysis at the site of colocalization of Cherry-4B1–261 and EGFP-ADRP. Unfortunately, definitive data have not been obtained, because of the time resolution constraints of our equipment. We think that further investigation is needed to prove our hypothesis.

Our imaging study also revealed that hydrophobic residues in amphipathic helices [43W, 46L (V in JFH1), 50W, 57F, 61I, and 64L in the N-terminal domain; 242V, 246L, 249L, and 253I in the C-terminal domain] were important for LD targeting of NS4B. Mutational study of these residues in JFH1 replication/infection system revealed their role in LD targeting by NS4B and the significance of LD targeting in replication of infectious virions. The cluster mutants (three or four residues simultaneously mutated to alanine) were defective in virus replication. The amphipathic helices are multifunctional; for example, they are involved in oligomerization of NS4B (31, 44), formation of membranous web (31, 44) and replication complex (31, 45), and membrane association (40, 41). Therefore, multiple inhibitory mechanisms may be acting in the cluster mutants to cause severe defects.

Examination of single alanine substitution mutants focused on the residues in the first cluster (W43, V46, and W50) and clarified their role in virus replication. The results from W43A and W50A mutants indicated that both tryptophan residues are critical for the production of infectious virions. In contrast to W43A, the W50A mutant severely impaired the expression of HCV antigens. This might have resulted from a severe defect in RNA replication, or the residue 50W might be involved in the synthesis or processing of HCV polyproteins or in protein stability, in addition to known functions in NS4B. The defective mutant W43A was key to demonstrating the relationship between the hydrophobic residues and LD targeting of NS4B and the significance of LD targeting in virus replication. As shown in Fig. 5, we could not detect LD association of W43A NS4B, indicating that disruption of LD association of NS4B resulted in reduced

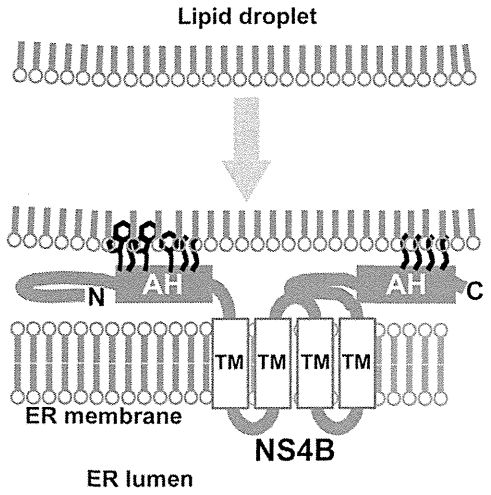

Fig. 6. Schematic representation of the hypothetical role of NS4B. NS4B tethers LDs on ER through the hydrophobic residues in the amphipathic helices (AH). N and C indicate the N- and C-terminal of NS4B, respectively. TM, transmembrane helix.

infectious virion release. This conclusion was supported by the results for V46A mutant, in which LD association of NS4B was apparently not affected and infectious virion release was comparable to that of wild-type JFH1. The residue 46V might not be important for LD targeting in strain JFH1.

In contrast to the JFH1 system, the impact of W43A mutation was unclear from the overexpression results using a truncated form of NS4B (Fig. 4). According to our model (Fig. 6), NS4B mediates association of LDs with ER membranes. When LDs move away from the site of association, a large force may act to disrupt the interaction between NS4B and LD membranes, and the residue 43W may be important to maintain the interaction as it is highly hydrophobic. The interactions of each of the hydrophobic residues involved in LD targeting depend on the adopted conformations of NS4B and those of molecules interacting with NS4B (HCV proteins, cellular proteins, or lipids); the changes in the mutual positioning of these molecules can induce steric hindrance. The 43W residue might be critical in such microenvironments. In contrast, the truncated form of NS4B (amino acids 1–73) may target LDs directly in a less regulated manner. This interaction may not be related to ER membranes and, hence, may not be affected by LD movements. The 43W residue influence is less than that of the intact NS4B.

We used an anti-NS4AB antibody; therefore, it remains to be resolved which antigens were observed in our imaging study (Fig. 5B and supplementary Fig. V). NS4A is a small protein consisting of 54 amino acids and is closely associated with NS3 to form NS3–4A complex. NS3–4A complex is thought to associate with ER membranes through the N-terminal hydrophobic α-helix of NS4A as a membrane anchor (46). Thus, it is unlikely that the W43A mutation of NS4B directly elicits solely the loss of association between NS3–4A and LDs as seen in Fig. 5B. At present, it is also not known whether the NS3–4A complex has an activity by itself to target LDs, although NS3 harbors an amphipathic helix α_0 that mediates membrane association (46). The most straightforward interpretation is that both NS4B and NS4A (and NS3) are present on ER membranes close to LDs, via the function of NS4B, and that W43A mutation causes loss of association with (or proximity to) LDs of both these proteins (but mostly NS4B).

The reason why LD targeting by NS4B is critical for virus replication is of interest. The microenvironment of LDs and ER membranes is thought to initiate HCV virion assembly, in which the nascent genome meets and associates with the Core protein to form nucleocapsids (10). Upon or after capsid formation, some particles may acquire an envelope (47), probably by utilizing ER membranes containing envelope proteins. Simultaneously, the virions might associate (or be coated) with components resembling VLDL, such as triglycerides, probably supplied from LDs, and apolipoproteins to become lipoviroparticles. Although the process of lipoviroparticle formation remains unclear, NS4B may function to establish such a microenvironment. NS4B can undergo a major conformational change, in which the N-terminal domain translocates to the luminal side of the ER (43), suggesting that the LD-targeting domain is masked by this event. The translocation was reduced in the presence of NS5A (48), suggesting a functional switch for NS4B. NS4B is indeed multifunctional because of its amphipathic helices, and in addition, it is thought to interact with other NS proteins (49), to hydrolyze GTP (50), and to modulate lipid metabolism (51). It is, therefore, of particular interest how, when, and where these activities have emerged and been regulated. A simple explanation may be that each activity simply emerges depending on the position or location of the NS4B molecule and what exists around it. The amphipathic helices of NS4B may function as ER anchors, as long as LDs are not present near the ER.

The authors thank Drs. K. Shimizu, Y. Shimotai, M. Hijikata, and T. Hayashida for valuable comments. Technical assistance by K. Toyosawa is gratefully acknowledged.

REFERENCES

1. Digel, M., R. Ehehalt, and J. Füllekrug. 2010. Lipid droplets lighting up: insights from live microscopy. *FEBS Lett.* **584:** 2168–2175.
2. Beller, M., K. Thiel, P. J. Thul, and H. Jäckle. 2010. Lipid droplets: a dynamic organelle moves into focus. *FEBS Lett.* **584:** 2176–2182.
3. Ohsaki, Y., J. L. Cheng, M. Suzuki, Y. Shinohara, A. Fujita, and T. Fujimoto. 2009. Biogenesis of cytoplasmic lipid droplets: From the lipid ester globule in the membrane to the visible structure. *Biochim. Biophys. Acta.* **1791:** 399–407.
4. Miyanari, Y., K. Atsuzawa, N. Usuda, K. Watashi, T. Hishiki, M. Zayas, R. Bartenschlager, T. Wakita, M. Hijikata, and K. Shimotohno. 2007. The lipid droplet is an important organelle for hepatitis C virus production. *Nat. Cell Biol.* **9:** 1089–1097.
5. Kato, N., M. Hijikata, Y. Ootsuyama, M. Nakagawa, S. Ohkoshi, T. Sugimura, and K. Shimotohno. 1990. Molecular cloning of the human hepatitis C virus genome from Japanese patients with non-A, non-B hepatitis. *Proc. Natl. Acad. Sci. USA.* **87:** 9524–9528.
6. Tsukiyama-Kohara, K., N. Iizuka, M. Kohara, and A. Nomoto. 1992. Internal ribosome entry site within hepatitis C virus RNA. *J. Virol.* **66:** 1476–1483.
7. Tanaka, T., N. Kato, M. J. Cho, and K. Shimotohno. 1995. A novel sequence found at the 3′ terminus of hepatitis C virus genome. *Biochem. Biophys. Res. Commun.* **215:** 744–749.

8. Tanaka, T., N. Kato, M. J. Cho, K. Sugiyama, and K. Shimotohno. 1996. Structure of the 3′ terminus of the hepatitis C virus genome. *J. Virol.* **70:** 3307–3312.
9. McLauchlan, J. 2009. Lipid droplets and hepatitis C virus infection. *Biochim. Biophys. Acta.* **1791:** 552–559.
10. Bartenschlager, R., F. Penin, V. Lohmann, and P. André. 2011. Assembly of infectious hepatitis C virus particles. *Trends Microbiol.* **19:** 95–103.
11. Negro, F. 2010. Abnormalities of lipid metabolism in hepatitis C virus infection. *Gut.* **59:** 1279–1287.
12. Herker, E., and M. Ott. 2011. Unique ties between hepatitis C virus replication and intracellular lipids. *Trends Endocrinol. Metab.* **22:** 241–248.
13. Ploss, A., and M. J. Evans. 2012. Hepatitis C virus host cell entry. *Curr. Opin. Virol.* **2:** 14–19.
14. Moriya, K., H. Yotsuyanagi, Y. Shintani, H. Fujie, K. Ishibashi, Y. Matsuura, T. Miyamura, and K. Koike. 1997. Hepatitis C virus core protein induces hepatic steatosis in transgenic mice. *J. Gen. Virol.* **78:** 1527–1531.
15. Moradpour, D., C. Englert, T. Wakita, and J. R. Wands. 1996. Characterization of cell lines allowing tightly regulated expression of hepatitis C virus core protein. *Virology.* **222:** 51–63.
16. Jirasko, V., R. Montserret, J. Y. Lee, J. Gouttenoire, D. Moradpour, F. Penin, and R. Bartenschlager. 2010. Structural and functional studies of nonstructural protein 2 of the hepatitis C virus reveal its key role as organizer of virion assembly. *PLoS Pathog.* **6:** e1001233.
17. Shi, S. T., S. J. Polyak, H. Tu, D. R. Taylor, D. R. Gretch, and M. M. Lai. 2002. Hepatitis C virus NS5A colocalizes with the core protein on lipid droplets and interacts with apolipoproteins. *Virology.* **292:** 198–210.
18. Roingeard, P., C. Hourioux, E. Blanchard, and G. Prensier. 2008. Hepatitis C virus budding at lipid droplet-associated ER membrane visualized by 3D electron microscopy. *Histochem. Cell Biol.* **130:** 561–566.
19. Christianson, J. L., E. Boutet, V. Puri, A. Chawla, and M. P. Czech. 2010. Identification of the lipid droplet targeting domain of the Cidea protein. *J. Lipid Res.* **51:** 3455–3462.
20. Hinson, E. R., and P. Cresswell. 2009. The antiviral protein, viperin, localizes to lipid droplets via its N-terminal amphipathic alpha-helix. *Proc. Natl. Acad. Sci. USA.* **106:** 20452–20457.
21. Poppelreuther, M., B. Rudolph, C. Du, R. Grossmann, M. Becker, C. Thiele, R. Ehehalt, and J. Fuellekrug. 2012. The N-terminal region of acyl-CoA synthetase 3 is essential for both the localization on lipid droplets and the function in fatty acid uptake. *J. Lipid Res.* **53:** 888–900.
22. Boulant, S., R. Montserret, R. G. Hope, M. Ratinier, P. Targett-Adams, J. P. Lavergne, F. Penin, and J. McLauchlan. 2006. Structural determinants that target the hepatitis C virus core protein to lipid droplets. *J. Biol. Chem.* **281:** 22236–22247.
23. Unterstab, G., R. Gosert, D. Leuenberger, P. Lorentz, C. H. Rinaldo, and H. H. Hirsch. 2010. The polyomavirus BK agnoprotein co-localizes with lipid droplets. *Virology.* **399:** 322–331.
24. Ingelmo-Torres, M., E. Gonzalez-Moreno, A. Kassan, M. Hanzal-Bayer, F. Tebar, A. Herms, T. Grewal, J. F. Hancock, C. Enrich, M. Bosch, et al. 2009. Hydrophobic and basic domains target proteins to lipid droplets. *Traffic.* **10:** 1785–1801.
25. Subramanian, V., A. Garcia, A. Sekowski, and D. L. Brasaemle. 2004. Hydrophobic sequences target and anchor perilipin A to lipid droplets. *J. Lipid Res.* **45:** 1983–1991.
26. Zehmer, J. K., R. Bartz, P. Liu, and R. G. Anderson. 2008. Identification of a novel N-terminal hydrophobic sequence that targets proteins to lipid droplets. *J. Cell Sci.* **121:** 1852–1860.
27. Gouttenoire, J., F. Penin, and D. Moradpour. 2010. Hepatitis C virus nonstructural protein 4B: a journey into unexplored territory. *Rev. Med. Virol.* **20:** 117–129.
28. Hügle, T., F. Fehrmann, E. Bieck, M. Kohara, H. G. Krausslich, C. M. Rice, H. E. Blum, and D. Moradpour. 2001. The hepatitis C virus nonstructural protein 4B is an integral endoplasmic reticulum membrane protein. *Virology.* **284:** 70–81.
29. Egger, D., B. Wölk, R. Gosert, L. Bianchi, H. E. Blum, D. Moradpour, and K. Bienz. 2002. Expression of hepatitis C virus proteins induces distinct membrane alterations including a candidate viral replication complex. *J. Virol.* **76:** 5974–5984.
30. Ferraris, P., E. Beaumont, R. Uzbekov, D. Brand, J. Gaillard, E. Blanchard, and P. Roingeard. Sequential biogenesis of host cell membrane rearrangements induced by hepatitis C virus infection. *Cell. Mol. Life Sci.* Epub ahead of print. November 25, 2012; doi:10.1007/s00018-012-1213-0.
31. Paul, D., I. Romero-Brey, J. Gouttenoire, S. Stoitsova, J. Krijnse-Locker, D. Moradpour, and R. Bartenschlager. 2011. NS4B self-interaction through conserved C-terminal elements is required for the establishment of functional hepatitis C virus replication complexes. *J. Virol.* **85:** 6963–6976.
32. Romero-Brey, I., A. Merz, A. Chiramel, J. Y. Lee, P. Chlanda, U. Haselman, R. Santarella-Mellwig, A. Habermann, S. Hoppe, S. Kallis, et al. 2012. Three-dimensional architecture and biogenesis of membrane structures associated with hepatitis C virus replication. *PLoS Pathog.* **8:** e1003056.
33. Wakita, T., T. Pietschmann, T. Kato, T. Date, M. Miyamoto, Z. Zhao, K. Murthy, A. Habermann, H. G. Krausslich, M. Mizokami, et al. 2005. Production of infectious hepatitis C virus in tissue culture from a cloned viral genome. *Nat. Med.* **11:** 791–796.
34. Ikeda, M., K. Abe, H. Dansako, T. Nakamura, K. Naka, and N. Kato. 2005. Efficient replication of a full-length hepatitis C virus genome, strain O, in cell culture, and development of a luciferase reporter system. *Biochem. Biophys. Res. Commun.* **329:** 1350–1359.
35. Naka, K., M. Ikeda, K. Abe, H. Dansako, and N. Kato. 2005. Mizoribine inhibits hepatitis C virus RNA replication: effect of combination with interferon-alpha. *Biochem. Biophys. Res. Commun.* **330:** 871–879.
36. Ohsaki, Y., T. Maeda, and T. Fujimoto. 2005. Fixation and permeabilization protocol is critical for the immunolabeling of lipid droplet proteins. *Histochem. Cell Biol.* **124:** 445–452.
37. Tanaka, T., T. Ito, M. Furuta, C. Eguchi, H. Toda, E. Wakabayashi-Takai, and K. Kaneko. 2002. In situ phage screening. A method for identification of subnanogram tissue components in situ. *J. Biol. Chem.* **277:** 30382–30387.
38. Fujimoto, Y., J. Onoduka, K. J. Homma, S. Yamaguchi, M. Mori, Y. Higashi, M. Makita, T. Kinoshita, J. Noda, H. Itabe, et al. 2006. Long-chain fatty acids induce lipid droplet formation in a cultured human hepatocyte in a manner dependent of Acyl-CoA synthetase. *Biol. Pharm. Bull.* **29:** 2174–2180.
39. Boleti, H., D. Smirlis, G. Dalagiorgou, E. F. Meurs, S. Christoforidis, and P. Mavromara. 2010. ER targeting and retention of the HCV NS4B protein relies on the concerted action of multiple structural features including its transmembrane domains. *Mol. Membr. Biol.* **27:** 50–74.
40. Gouttenoire, J., R. Montserret, A. Kennel, F. Penin, and D. Moradpour. 2009. An amphipathic alpha-helix at the C terminus of hepatitis C virus nonstructural protein 4B mediates membrane association. *J. Virol.* **83:** 11378–11384.
41. Gouttenoire, J., V. Castet, R. Montserret, N. Arora, V. Raussens, J. M. Ruysschaert, E. Diesis, H. E. Blum, F. Penin, and D. Moradpour. 2009. Identification of a novel determinant for membrane association in hepatitis C virus nonstructural protein 4B. *J. Virol.* **83:** 6257–6268.
42. Turró, S., M. Ingelmo-Torres, J. M. Estanyol, F. Tebar, M. A. Fernandez, C. V. Albor, K. Gaus, T. Grewal, C. Enrich, and A. Pol. 2006. Identification and characterization of associated with lipid droplet protein 1: A novel membrane-associated protein that resides on hepatic lipid droplets. *Traffic.* **7:** 1254–1269.
43. Lundin, M., M. Monné, A. Widell, G. Von Heijne, and M. A. Persson. 2003. Topology of the membrane-associated hepatitis C virus protein NS4B. *J. Virol.* **77:** 5428–5438.
44. Gouttenoire, J., P. Roingeard, F. Penin, and D. Moradpour. 2010. Amphipathic alpha-helix AH2 is a major determinant for the oligomerization of hepatitis C virus nonstructural protein 4B. *J. Virol.* **84:** 12529–12537.
45. Aligo, J., S. A. Z. Jia, D. Manna, and K. V. Konan. 2009. Formation and function of hepatitis C virus replication complexes require residues in the carboxy-terminal domain of NS4B protein. *Virology.* **393:** 68–83.
46. Brass, V., J. M. Berke, R. Montserret, H. E. Blum, F. Penin, and D. Moradpour. 2008. Structural determinants for membrane association and dynamic organization of the hepatitis C virus NS3-4A complex. *Proc. Natl. Acad. Sci. USA.* **105:** 14545–14550.
47. Gastaminza, P., K. A. Dryden, B. Boyd, M. R. Wood, M. Law, M. Yeager, and F. V. Chisari. 2010. Ultrastructural and biophysical characterization of hepatitis C virus particles produced in cell culture. *J. Virol.* **84:** 10999–11009.
48. Lundin, M., H. Lindström, C. Grönwall, and M. A. Persson. 2006. Dual topology of the processed hepatitis C virus protein NS4B is influenced by the NS5A protein. *J. Gen. Virol.* **87:** 3263–3272.
49. Dimitrova, M., I. Imbert, M. P. Kieny, and C. Schuster. 2003. Protein-protein interactions between hepatitis C virus nonstructural proteins. *J. Virol.* **77:** 5401–5414.
50. Einav, S., M. Elazar, T. Danieli, and J. S. Glenn. 2004. A nucleotide binding motif in hepatitis C virus (HCV) NS4B mediates HCV RNA replication. *J. Virol.* **78:** 11288–11295.
51. Park, C. Y., H. J. Jun, T. Wakita, J. H. Cheong, and S. B. Hwang. 2009. Hepatitis C virus nonstructural 4B protein modulates sterol regulatory element-binding protein signaling via the AKT pathway. *J. Biol. Chem.* **284:** 9237–9246.

ARTICLE
Journal of Cellular Biochemistry 114:1987–1996 (2013)

Journal of Cellular Biochemistry

Suppressive Effect of the Histone Deacetylase Inhibitor Suberoylanilide Hydroxamic Acid (SAHA) on Hepatitis C Virus Replication

Ayami Sato,[1] Yoshimasa Saito,[1,2] Kazuo Sugiyama,[2] Noriko Sakasegawa,[1] Toshihide Muramatsu,[1] Shinya Fukuda,[1] Mikiko Yoneya,[1] Masaki Kimura,[1] Hirotoshi Ebinuma,[2] Toshifumi Hibi,[2] Masanori Ikeda,[3] Nobuyuki Kato,[3] and Hidetsugu Saito[1,2]*

[1]*Division of Pharmacotherapeutics, Keio University Faculty of Pharmacy, Tokyo, 1058512, Japan*
[2]*Department of Internal Medicine, Keio University School of Medicine, Tokyo, 1608582, Japan*
[3]*Department of Molecular Biology, Okayama University Graduate School of Medicine and Dentistry, Okayama, 7008558, Japan*

ABSTRACT

The histone deacetylase (HDAC) inhibitor suberoylanilide hydroxamic acid (SAHA) has a clinical promise for treatment of cancer including hepatocellular carcinoma (HCC). To investigate effect of SAHA on hepatitis C virus (HCV) replication, we treated the HCV replicon cell OR6 with SAHA. HCV replication was significantly inhibited by SAHA at concentrations below 1 μM with no cellular toxicity. Another HDAC inhibitor, tricostatin A, also showed reduction of HCV replication. The microarray analysis and quantitative RT-PCR demonstrated up-regulation of *osteopontin* (*OPN*) and down-regulation of *apolipoprotein-A1* (*Apo-A1*) after SAHA treatment. Direct gene induction of *OPN* and knockdown of *Apo-A1* also showed reduction of HCV replication. The liver specific *microRNA-122*, which is involved in HCV replication, was not affected by SAHA treatment. These results suggest that SAHA has suppressive effect on HCV replication through alterations of gene expression such as *OPN* and *Apo-A1* in host cells. Epigenetic treatment with HDAC inhibitors may be a novel therapeutic approach for diseases associated with HCV infection such as chronic hepatitis, liver cirrhosis, and HCC. J. Cell. Biochem. 114: 1987–1996, 2013.

KEY WORDS: SUBEROYLANILIDE HYDROXAMIC ACID; HEPATITIS C VIRUS; OR6; *MIR-122*; *OSTEOPONTIN*; *APOLIPOPROTEIN-A1*

Hepatitis C virus (HCV) infection is a major worldwide health problem and approximately 170 million people are infected with the virus. Roughly 60–80% of who carry HCV progress to chronic infection, in which liver cirrhosis and hepatocellular carcinoma (HCC) are frequent complications [Lauer and Walker, 2001]. Treatment of HCV infection has been progressed with introduction of protease inhibitors. Although the combination therapy with pegylated interferon (PEG-IFN), ribavirin, and protease inhibitors has shown a higher sustained virological response (SVR) rate, the SVR rate of patients with genotype 1b and a high viral load has not been satisfactory [Ikeda et al., 2006; Ebinuma et al., 2012; Takayama et al., 2011]. Effective drugs without severe side effects are needed for treatment of chronic infection with HCV genotype 1b.

HCV itself cannot replicate or proliferate with its own protein and nucleic acids, and instead relies on various host factors [Tu et al., 1999; Gao et al., 2004; Hamamoto et al., 2005; Okamoto et al., 2006]. It is possible to attenuate viral replication by stimulating some of these host factors [Kaul et al., 2009; Chen et al., 2010; Vaillancourt et al., 2012]; one such possibility involves epigenetic alterations. Epigenetics is an acquired modification of methylation and/or acetylation of chromatin DNA or histone proteins, which regulates downstream gene expression. Epigenetic alterations can be induced by aging, chronic inflammation, or viral infection.

Disclosure Statement: No conflicts of interest exist.
Grant sponsor: The Japan Society for the Promotion of Science (JSPS); Grant sponsor: Grant-in-Aid for Young Scientists A; Grant number: 23680090; Grant sponsor: Grant-in-Aid for Scientific Research C; Grant number: 24590993; Grant sponsor: Keio Gijuku Academic Development Fund; Grant sponsor: Takeda Science Foundation; Grant sponsor: Inaida Foundation.
*Correspondence to: Hidetsugu Saito, MD, PhD, Division of Pharmacotherapeutics, Keio University Faculty of Pharmacy, 1-5-30 Shiba-kohen, Minato-ku, Tokyo 1058512, Japan. E-mail: hsaito@a2.keio.jp
Manuscript Received: 16 August 2012; Manuscript Accepted: 5 March 2013
Accepted manuscript online in Wiley Online Library (wileyonlinelibrary.com): 20 March 2013
DOI 10.1002/jcb.24541 • © 2013 Wiley Periodicals, Inc.

Aberrations in DNA methylation and histone modification may induce inactivation of tumor suppressor genes and play critical roles in the initiation and progression of human cancer [Gal-Yam et al., 2008]. Moreover, a recent study has demonstrated that the liver-specific microRNA (miRNA) *miR-122* binds to the 5′ noncoding region of the HCV genome and facilitates HCV replication [Jopling et al., 2005; Sarasin-Filipowicz et al., 2009]. MiRNAs are small non-coding RNAs that function as endogenous silencers of various target genes and are expressed in a tissue-specific manner. MiRNAs play important roles in cell proliferation, apoptosis, and differentiation [Schickel et al., 2008]. We have recently reported that some miRNAs are regulated by epigenetic alterations such as DNA methylation and histone modification at their CpG island promoters [Saito et al., 2006].

Unlike genetic alterations, which are almost impossible to reverse, epigenetic aberrations are potentially reversible, allowing the malignant cell population to revert to a more normal state [Kurita et al., 2010]. Chromatin-modifying drugs such as DNA methylation inhibitors and histone deacetylase (HDAC) inhibitors have clinical promise for cancer therapy [Yoo and Jones, 2006]. The HDAC inhibitor suberoylanilide hydroxamic acid (SAHA) is emerging as a promising agent for epigenetic therapy of human malignancies including HCC [Butler et al., 2002]. SAHA was recently approved in Japan for the treatment of cutaneous T-cell lymphoma [Watanabe et al., 2010].

In the present study, we investigated the effect of SAHA on HCV RNA replication in the replicon cell OR6, in which genotype 1b full-length HCV RNA replicates and HCV RNA replication can be monitored by luciferase reporter assay [Ikeda et al., 2005]. Here we show that SAHA has a suppressive effect on HCV replication through changes of gene expression in OR6 cells, suggesting that HDAC inhibitors could be promising drugs for diseases associated with chronic HCV infection.

MATERIALS AND METHODS

CELL CULTURE

OR6 cells were cultured in Dulbecco's modified Eagle's medium (DMEM; Gibco) with 4.5 g/L glucose (Gibco) with 10% heat inactivated fetal bovine serum (FBS; BioWest), 1% penicillin-streptomycin solution (Sigma-Aldrich Japan, Tokyo), and 50 mg/ml G-418 (Roche Diagnostics Co.) in 5% CO_2 in humidified air at 37°C as described previously [Nakamura et al., 2008].

SAHA AND TRICHOSTATIN A (TSA) TREATMENT

SAHA (Sigma-Aldrich) and TSA (Sigma-Aldrich) were dissolved in dimethylsulphoxide (DMSO, Sigma-Aldrich) and ethanol, respectively, and added to culture medium. As a control, DMSO or ethanol diluted with culture medium was used.

MTT ASSAY

Cell proliferation was also measured using the MTT Cell Proliferation Assay Kit (Cayman Chemical). OR6 cells were seeded at 1.0×10^4 cells/well in a 96-well plate and cultured for 24 h. SAHA (0.1, 0.5, 1.0, 1.5, 3.0, and 5 μM) was added and the cells were further cultured for 72 h. MTT reagent (10 μM) was added to each well and the plate was the shaken for 1 min and subsequently incubated at 37°C for 3 h. A sample from each well was mixed with 100 μl Crystal Dissolving solution and shaken for 30 min, and the absorption was measured at 570 nm.

CELL NUMBER COUNTING

OR6 cells were seeded at 1.0×10^5 cells/well in a 6-well plate, and 1.0 μM of SAHA was added after 24 h and the cells were then cultured for 72 h. Cells were collected after treating with trypsin (Sigma-Aldrich) and number of cells number was counted using a hemocytometer and the Scepter 2.0 Handheld Cell Counter (Millipore).

CELL VIABILITY ASSAY

The viability of OR6 cells treated with SAHA was analyzed using Vi-CELL XR cell viability counter (Beckman Coulter). Five hundred microliters of cell suspension were mixed with trypan blue, and then images were taken to determine cell concentration and viability.

LUCIFERASE ASSAY

OR6 cells were seeded at 4.0×10^4 cells/well in a 24-well plate for 24 h. SAHA (0.1, 0.5, 0.8, or 1.0 μM) was added and the cells were then cultured for 72 h. Luciferase activity was measured with Renilla Luciferase Assay System (Promega) using a luminometer (Lumat CB 9507, Berthold Technologies). One hundred microliters of Renilla Luciferase Assay Reagent and 20 μl of cell lysate were mixed in tube, and then luminescence was measured. Luciferase activity was normalized with cell number.

RNA EXTRACTION

Total RNA including small RNA was extracted from OR6 cells using the mirVana miRNA isolation kit (Ambion). The sample is first lysed in a denaturing lysis solution which stabilizes RNA and inactivates RNases. The lysate is then extracted once with Acid-Phenol: Chloroform which removes most of the other cellular components, leaving a semi-pure RNA sample. This is further purified over a glass-fiber filter to yield total RNA enriched in miRNAs.

QUANTITATIVE RT-PCR OF *miR-122*

Levels of miRNA expression were analyzed by quantitative RT-PCR using the TaqMan microRNA assay for *miR-122* (Applied Biosystems) according to the manufacturer's instructions. Expression levels were normalized to that of U6 RNA.

MICROARRAY ANALYSIS

Microarray analysis was carried out using the Human Oligo chip 25K (ID QH0ZG35) by Toray (http://www.3d-gene.com/). In brief, total RNA was amplified using an Amino Allyl aRNA kit (Ambion). RNA from SAHA treated cells was labeled with Cy3 Mono-Reactive Dye (GE Healthcare), and control RNA was labeled with Cy5 Mono-Reactive Dye (GE Healthcare). After purification, each 1 μg sample was mixed and hybridized at 37°C for 16 h. After washing, the hybridized chip was scanned using a 3D-Gene Scanner 3000 (Toray). Background was subtracted from the raw data and the values were normalized according to a median Cy3/Cy5 ratio of 1.

QUANTITATIVE RT-PCR OF *OPN* AND *Apo-A1*

After incubation with DNase I (Promega) to eliminate DNA contamination, 1 mg of total RNA was applied for RT reaction with random primers using High Capacity cDNA Reverse Transcription kit (Applied Biosystems). Then, quantitative RT-PCR was performed with

SYBR Green PCR Master Mix (Applied Biosystems) using CFX96 real-time PCR system (Bio-Rad). The primer sequences for quantitative RT-PCR of *OPN* and *Apo-A1* were obtained from the previous reports [Hahnel et al., 2010; Haas et al., 2011]. *GAPDH* was used as an internal control.

OPN forward: 5′-TGGCCGAGGTGATAGTGTG-3′, *OPN* reverse: 5′-CGGGGATGGCCTTGTATG-3′, *Apo-A1* forward: 5′-AGCTTGCT-GAAGGTGGAGGT-3′, *Apo-A1* reverse: 5′-ATCGAGTGAAGGACC-TGGC-3′, *GAPDH* forward: 5′-CTCCTCCTGTTCGACAGTCAGC-3′, *GAPDH* reverse: 5′-CCCAATACGACCAAATCCGTTG-3′.

The PCR conditions were as follows; *OPN*: 95°C for 15 min, 40-cycles following reaction; 95°C for 30 s, 60°C for 30 s, and 72°C for 30 s. *Apo-A1*: 95°C 3 min, 40 cycles; 95°C for 1 min, 52°C for 1 min, and 72°C for 1 min.

WESTERN BLOTTING OF OPN AND Apo-A1

Protein extracts were separated by SDS/polyacrylamide gel electrophoresis and transferred onto nitrocellulose membranes. Membranes were hybridized with the mouse anti-OPN monoclonal antibody (sc-21742, Santa Cruz Biotechnology) and the goat anti-Apo-A1 polyclonal antibody (ab7613, Abcam). β-actin was used as the internal control.

CHROMATIN IMMUNOPRECIPITATION (ChIP) ASSAY

ChIP assay for acetylation of histone H3 around the promoter region of *OPN* was performed using acetyl-histone H3 ChIP assay kit (Millipore) according to the manufacturer's instructions. In brief, 1×10^7 of OR6 cells were cross-linked with 1% formaldehyde at 37°C for 10 min. Crude cell lysates were sonicated to generate DNA fragments of 200–1,000 bp. ChIP was performed with anti-acetyl-histone H3 antibody as well as control IgG. Quantitative PCR analysis was performed with SYBR Green PCR Master Mix (Applied Biosystems) using a CFX96 real-time PCR system (Bio-Rad). The primer sequence for ChIP assay of *OPN* was designed using the UCSC Genome Browser (http://genome.ucsc.edu/) and the Primer3 (http://frodo.wi.mit.edu/).

OPN (ChIP) forward: 5′-TCATACAGGCAAGAGTGGTTGCAGA-3′, *OPN* (ChIP) reverse: 5′-GCTCCCACACTTCCCCCTCTGGTTT-3′.

The primer sequence for ChIP assay of *Apo-A1* was obtained from the previous report [Mishiro et al., 2009].

Apo-A1 (ChIP) forward: 5′-CAAGGCCTGAACCTTGAGC-3′, *Apo-A1* (ChIP) reverse: 5′-TTAGAGACTGCGAGAAGGAGGT-3′.

The PCR conditions were as follows; 95°C for 3 min, 40-cycles following reaction; 95°C for 30 s, 60°C for 30 s, and 72°C for 30 s. The fraction of immunoprecipitated DNA was calculated as follows: [immunoprecipitated DNA (IP) with anti-acetyl-histone H3 antibody–nonspecific antibody control (NAC)]/(input DNA–NAC). Fold changes relative to control that was set to 1.0 were compared.

TRANSFECTION OF THE *OPN* EXPRESSION VECTOR AND THE *Apo-A1* siRNA

The expression vector containing the *OPN* open reading flame and the pre-designed siRNA for the *Apo-A1* gene (#s1467) were purchased from InvivoGen and Ambion, respectively. They were transfected into OR6 cells using lipofectamine (Invitrogen) in accordance with the manufacturer's instructions. Forty-eight hours after transfection, the cells were collected and luciferase activity was analyzed as described above. OR6 cells treated with lipofectamine only were used as controls.

STATISTICS

The data were expressed as mean and standard deviation (SD) for at least three independent experiments. The data were analyzed using the SPSS statistics software and differences with P values of less than 0.05 were considered significant.

RESULTS

TREATMENT OF OR6 CELLS WITH 1.0 MM OF SAHA DID NOT AFFECT CELL VIABILITY

To investigate the cellular toxicity of SAHA in OR6 cells, MTT assay was performed, and the results showed no significant difference in absorbance at concentrations less than 1.5 μM of SAHA, whereas the absorbance at 3 and 5 μM was significantly reduced ($P < 0.01$, Fig. 1A).

We next examined cell number and cell viability after treatment with SAHA using Scepter Handheld Cell Counter and Vi-CELL autoanalyzer, respectively. Cell viability did not differ after treatment with 1.0 μM of SAHA for 72 h as compared to control (Fig. 1B). We also confirmed that there was no significant difference in cell number among control cells and cells treated with 1.0 μM of SAHA and 0.1 μM of another HDAC inhibitor TSA for 24, 48, and 72 h (Fig. 1C). These findings indicate that treatment with SAHA at concentration of 1.0 μM for 72 h did not affect the viability of OR6 cells.

TREATMENT OF OR6 CELLS WITH SAHA AND TSA REDUCED HCV REPLICATION

We next evaluated HCV replication by measuring luciferase activity in OR6 cells. Luciferase activity of OR6 cells was measured after treatment with SAHA at concentrations of 0.1, 0.5, 0.8, or 1.0 μM for 72 h. As shown in Figure 2A, treatment of OR6 cells with SAHA (<1.0 μM) reduced luciferase activity in a dose-dependent manner. Treatment with SAHA at concentrations of 1.0 and 0.8 μM significantly reduced luciferase activity compared to control (Fig. 2A, 1.0 μM: $P < 0.01$, 0.8 μM: $P < 0.05$).

To investigate whether the effect of SAHA was agent-specific or a general consequence of HDAC inhibitors, we treated OR6 cells with another HDAC inhibitor TSA at concentrations of 0.1 and 0.5 μM and confirmed that TSA also suppresses HCV replication (Fig. 2B).

LACK OF INVOLVEMENT OF *miR-122* IN THE SUPPRESSIVE EFFECT OF SAHA ON HCV REPLICATION

The liver-specific miRNA *miR-122* has been reported to bind to the 5′ noncoding region of the HCV genome to facilitate replication of the viral RNA [Jopling et al., 2005]. To determine whether the suppressive effect of HDAC inhibitors on HCV replication is mediated through alterations in *miR-122* expression, we performed quantitative RT-PCR to measure *miR-122* expression in OR6 cells cultured with 1 μM SAHA or 0.1 μM TSA for 72 h. As shown in Figure 3, *miR-122* expression did not differ between control cells and cells treated with

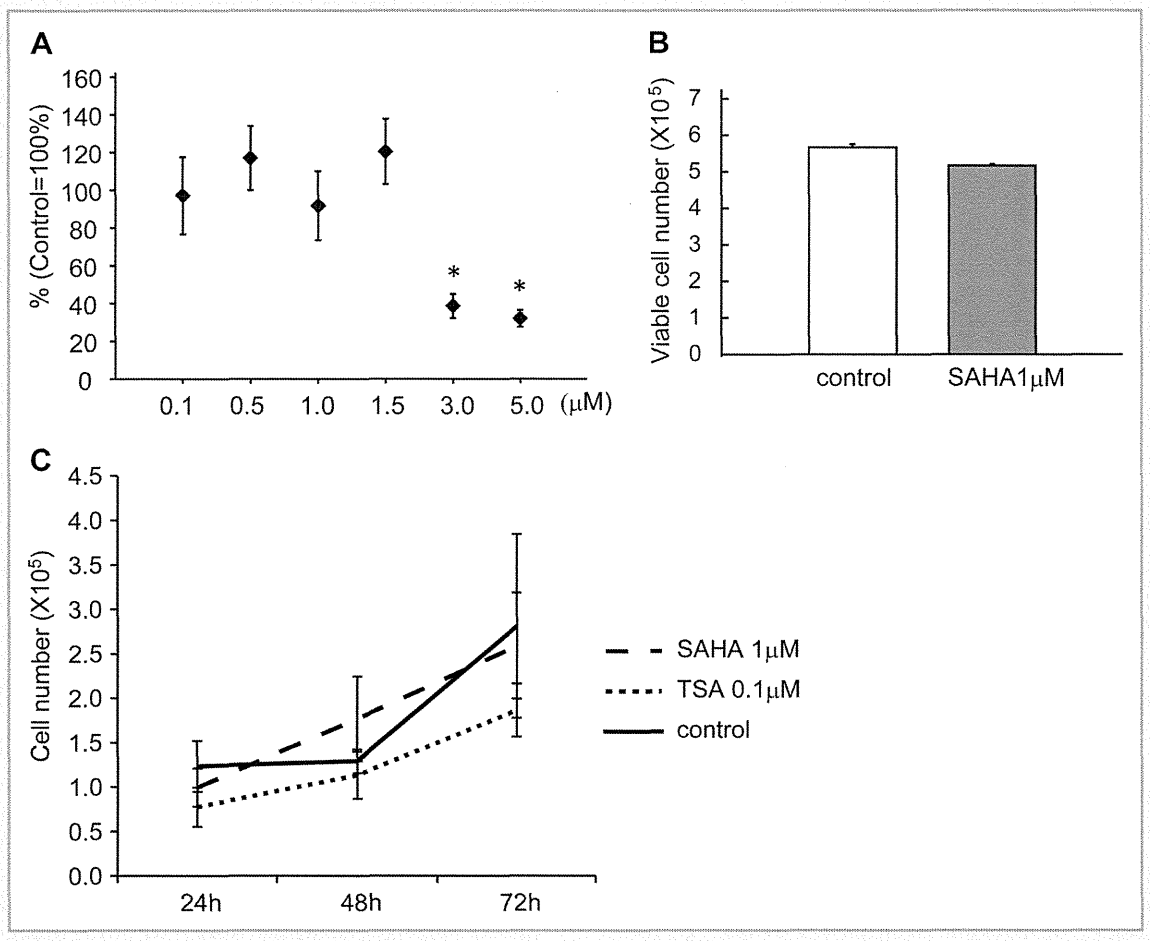

Fig. 1. A: MTT assay for cell viability of OR6 cells after SAHA treatment The viability of OR6 cells was measured by MTT assay. OR6 cells were treated with SAHA at concentrations of 0.1, 0.5, 1.0, 1.5, 3.0, or 5.0 μM for 72 h and MTT assay was then performed to determine the number of viable cells. Absorbance of cells treated with 3.0 and 5.0 μM of SAHA was significantly decreased compared with control. No toxic effect was observed at SAHA concentrations at or below 1 μM. Dots and bar indicate means and SDs for four experiments. *$P < 0.01$. B: Cell viability of OR6 cells after SAHA treatment OR6 cells were treated with 1 μM SAHA for 72 h. Cell viability was tested using a Vi-CELL autoanalyzer. There was no significant difference in the number of viable cells between the control and 1.0 μM SAHA conditions. Means and SDs of viable cell numbers for three experiments are shown. C: Cell number of OR6 cells treated with 1.0 μM SAHA and 0.1 μM TSA The cell number in OR6 cells treated with 1.0 μM SAHA and 0.1 μM TSA for 24, 48 and 72 h did not differ significantly versus control cells. Cell number was measured by the Scepter Handheld Cell Counter and means and SDs for five experiments are shown.

SAHA or TSA, indicating that *miR-122* is not involved in the suppressive effect of HDAC inhibitors on HCV replication.

ALTERATION OF *OSTEOPONTIN* (*OPN*) AND *APOLIPOPROTEIN-A1* (*Apo-A1*) EXPRESSION LEVELS AFTER TREATMENT OF OR6 CELLS WITH SAHA

To determine comprehensive gene expression changes induced by SAHA treatment, microarray analysis was applied in SAHA-treated OR6 cells (Fig. 4A). We selected genes with expression levels of more than 100 and more than a fourfold difference relative to control. The genes that were up-regulated and down-regulated in SAHA-treated OR6 cells are summarized in Tables I and II. Among genes whose expression was largely changed, we selected genes intimately related to HCV replication from Tables I and II by means of document retrieval. From the literature search, *OPN* was picked-up from the up-regulated genes since *OPN* is an important cytokine for host resistance to viral infection through the initiation of the Th1 immune response [Patarca et al., 1993; Ashkar et al., 2000]. *Apo-A1* was selected from among the down-regulated genes since *Apo-A1* is closely involved in the HCV life cycle [Mancone et al., 2011].

Quantitative RT-PCR shown in Figure 4B and C demonstrated that expression of *OPN* was significantly up-regulated (8.6-fold, $P < 0.001$), and expression of *Apo-A1* was significantly down-regulated (0.39-fold, $P < 0.001$) by treatment with 1 μM SAHA for 72 h. We confirmed the increased protein expression of OPN and the decreased protein expression of Apo-A1 after treatment with 1 μM SAHA by Western blotting (Fig. 4B,C). To investigate whether the changes in expression of these two genes affect HCV RNA replication in OR6 cells, we overexpressed the *OPN* gene using the expression vector containing the *OPN* open reading frame and knocked down the *Apo-A1* gene using the specific siRNA in OR6 cells and examined

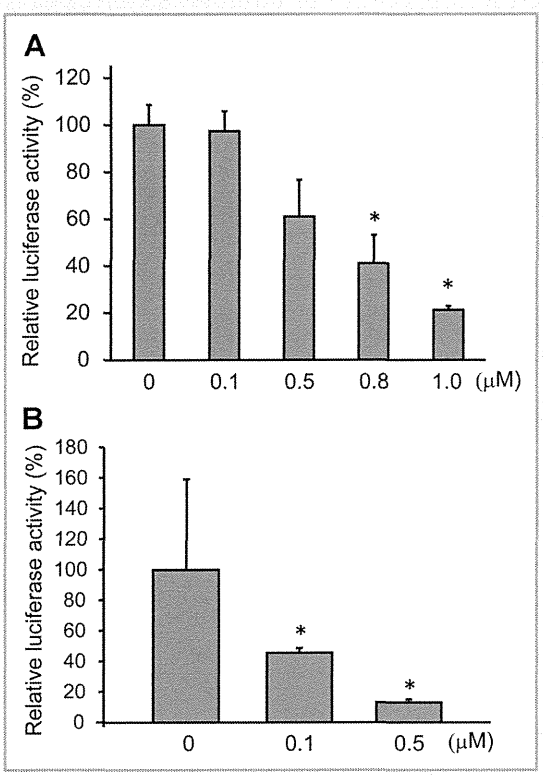

Fig. 2. A: HCV replication in OR6 cells after SAHA treatment HCV replication was evaluated by luciferase activity in OR6 cells treated with SAHA. OR6 cells were treated with 0.1, 0.5, 0.8, or 1.0 μM SAHA for 72 h and luciferase activity was measured. Means and SDs of luciferase activities for three experiments are shown. Luciferase activity in SAHA-treated OR6 cells was dose-dependently reduced, and the reduction at concentrations of 0.8 and 1.0 μM were statistically significant. *$P < 0.05$. B: HCV replication in OR6 cells after TSA treatment HCV replication was evaluated by luciferase activity in OR6 cells treated with TSA. Means and SDs of luciferase activities for three experiments are shown. OR6 cells were treated with 0.1 and 0.5 μM TSA, and the luciferase activity in TSA-treated OR6 cells was significantly reduced. *$P < 0.05$.

changes in luciferase activity. As shown in Figure 5A,B, we confirmed overexpression of OPN and knockdown of Apo-A1 after transfection of *OPN*-expressing vector and siRNA for *Apo-A1*, respectively. After transfection of *OPN*-expressing vector, luciferase activity was significantly reduced to around 40% of control ($P < 0.01$), and knockdown of *Apo-A1* by siRNA resulted in decrease of luciferase activity to around 60% of control ($P < 0.05$).

INCREASED HISTONE H3 ACETYLATION AT THE PROMOTER REGIONS OF *OPN* AND *Apo-A1* AFTER TREATMENT OF OR6 CELLS WITH SAHA

Since histone acetylation generally activates gene expression, we further examined histone acetylation levels around the promoter regions of *OPN* and *Apo-A1* by ChIP assay in OR6 cells treated with 1 μM SAHA.

We designed the ChIP primers according to the report of Liang et al. [2004]. They have demonstrated that histone H3 acetylation is localized within 500 bp of transcriptional start sites (TSSs) of transcriptionally active genes. Therefore we designed the ChIP primers within 500 bp of TSSs of the *OPN* gene and the *Apo-A1* gene, and confirmed the location of the ChIP primers using the UCSC Genome Browser (http://genome.ucsc.edu/). The ChIP-PCR products for the *OPN* gene and the *Apo-A1* gene are 279 and 78 bp, respectively (Fig. 6A,B).

The results of the ChIP assay showed that histone H3 acetylation levels of the promoter regions of *OPN* and *Apo-A1* were significantly higher in SAHA-treated OR6 cells compared to control ($P < 0.01$, Fig. 6A,B). These results suggest that up-regulation of the *OPN* gene is induced by histone H3 acetylation around its promoter region through SAHA treatment of OR6 cells. Although expression level of *Apo-A1* was significantly decreased after SAHA treatment of OR6 cells, histone H3 acetylation level of the promoter region of *Apo-A1* was increased after SAHA treatment.

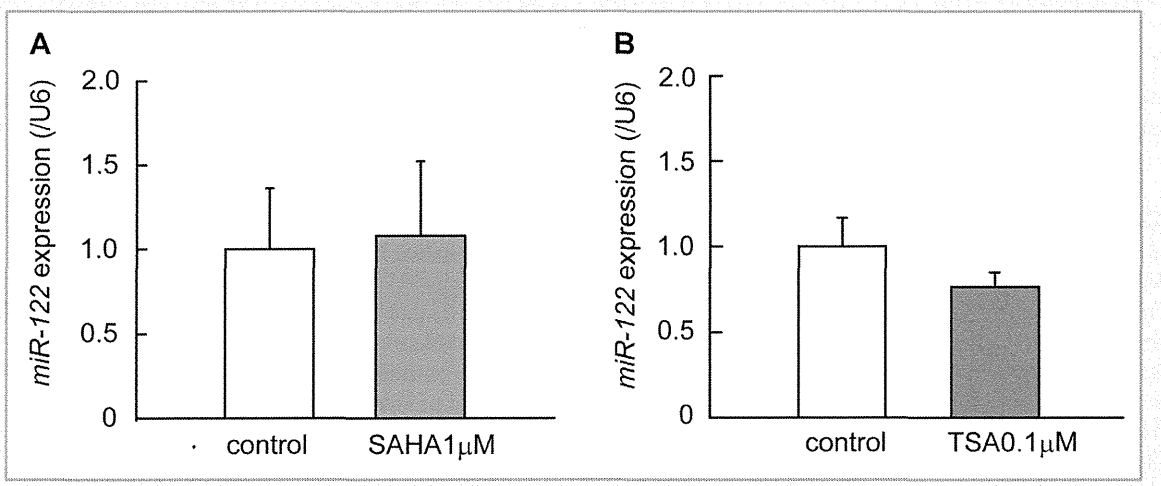

Fig. 3. Expression of *miR-122* in OR6 cells after treatment with SAHA and TSA OR6 cells were treated with 1 μM SAHA (A) or 0.1 μM TSA (B) for 72 h. Expression levels of *miR-122* were examined by TaqMan® quantitative RT-PCR. Means and SDs of *miR-122* expression normalized with U6 for three experiments are shown. There was no significant difference in *miR-122* expression between control and treatment with SAHA or TSA.